Wegener Center for Climate and Global Change
University of Graz
Atmospheric Remote Sensing and Climate System Research Group
ARSCliSys - on the art of understanding the climate system

WegCenter/UniGraz Technical Report for ESA/ESTEC No. 5/2007

Project:

Prodex-CN1 — Advanced Topics in RO Modelling and Retrieval
(Complementary Report)

Retrieval of Complex Refractivity, Temperature, and Humidity from Radio Occultation Data in X/K Band

by

Michael E. Gorbunov[1,3], Stephen S. Leroy[2], and Gottfried Kirchengast[3]

[1] A. M. Obukhov Institute of Atmospheric Physics, Moscow, Russia

[2] Harvard University, Cambridge MA, USA

[3] Wegener Center and IGAM/Inst. of Physics, University of Graz, Graz, Austria

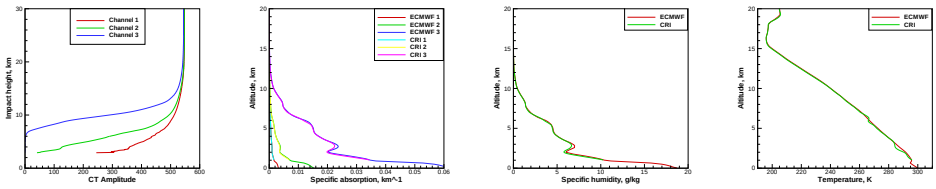

October 2007

Retrieval of Complex Refractivity, Temperature, and Humidity from Radio Occultation Data in X/K Band

M. E. Gorbunov[1,3], S. S. Leroy[2], and G. Kirchengast[3]

[1] A. M. Obukhov Institute of Atmospheric Physics, Moscow, Russia
[2] Harvard University, Cambridge, MA, USA
[3] Wegener Center and IGAM/Inst. of Physics, University of Graz, Graz, Austria

Abstract

The GPS radio occultation technique allows for the remote sensing of atmospheric refractivity. In the L band, which is used by GPS, the imaginary part of refractivity, although detectable, is small and cannot be accurately retrieved. Typical attenuation is about 1–2 dB, in the lowest troposphere, which is comparable with measurement errors. The real part of refractivity is a function of 3 variables: pressure, temperature, and humidity. The retrieved profile of refractivity together with the hydrostatic equation provides only 2 equations, which are insufficient for the retrieval of 3 main thermodynamic variables without additional information or constraints. The use of X/K frequencies changes the situation. The absorption in this band is much stronger than in L band and is characterized by a strong dependence on humidity. Given LEO–LEO occultation data for frequencies on the wing of the water vapor absoption line between 9 and 23 GHz, it becomes possible to formulate the problem of thermodynamic state retrieval. In this report we describe a basic algorithm for the retrieval of pressure, temperature and humidity from occultation data in X/K band. The wave-optical retrieval of atmospheric transmission and complex refractivity has been developed and described earlier. However, the last step of the complex refractivity inversion for the thermodynamic state retrieval proved to be difficult. Our approach is based on the downward integration of the hydrostatic equation with pressure being an independent variable. Temperature and humdity can then be expressed as functions of the retrieved complex refractivity and pressure, complemented with the a posteriori error estimates of observations and a priori error estimates of the unknown thermodynamic state variables. Additional constraint for the temperature gradient is added to stabilize the retrieval. We perform numerical simulations with global fields from ECMWF operational analyses. The simulations include wave-optical realistic forward modeling with subsequent inversion of the artificial occultation data. We show that, given this basic algorithm, humdity can be retrieved with sufficient accuracy.

1 Introduction

GPS radio occultations (RO) proved to be a very effective means for the remote sounding of the Earth's atmosphere for the purposes of numerical weather prediction (NWP) and climate monitoring. However, it has also been recognized that the GPS RO technique has a significant limitation: without a priori information it is impossible to separate the inputs of humidity and dry air into the overall refractive index. To overcome this limitation, different 1DVar, 2DVar, and 3DVar schemes of the assimilation of RO data into NWP models have been developed and utilized (*Eyre*, 1994; *Zou et al.*, 1999; *Gorbunov and Kornblueh*, 2003; *Liu and Zou*, 2003; *Engeln et al.*, 2003; *Healy et al.*, 2007).

Another more advanced solution implies launching a system of low-Earth orbiters (LEO) equipped with transmitters and receivers for the X/K band (*Kursinski et al.*, 2002; *Lohmann et al.*, 2003b; *Kirchengast and Høeg*, 2004; *Kirchengast et al.*, 2004). Given a set of frequency channels located at the wing of the water vapor absorption line (9–23 GHz), it is possible to retrieve temperature and humidity profiles without employing a priori information, because the water vapor component of the refractive index, unlike its dry part, indicates a strong dispersion in this band. The measurements of the amplitude of RO signals start playing a crucial role in this scheme. The amplitude is linked to the integral absorption along the ray, which is equal to the integral of the imaginary part of the refractive index. Therefore, the imaginary parts of the refractivity for each frequency channel can be retrieved in a way similar to the real refractivity retrieval, by the Abel inversion of the absorption profile.

In the framework of the geometric optical approximation, the integral absorption can be obtained as the logarithmic ratio of the measured amplitude and the refractive amplitude. The latter can be obtained from the bending angle profile by utilizing the energy conservation in each ray tube. The bending angle profile is derived from the phase measurements (*Kirchengast and Høeg*, 2004; *Kirchengast et al.*, 2004).

Wave optical algorithms including Canonical Transform (CT/CT2) (*Gorbunov*, 2002a; *Gorbunov and Lauritsen*, 2004), Full Spectrum Inversion (FSI) (*Jensen et al.*, 2003), and Phase Matching (PM) (*Jensen et al.*, 2004) can account for multipath propagation and diffraction effects. These methods allow for the derivation both of the bending angle profile and the absorption profiles. It was first observed by *Gorbunov* (2002a) that the CT-amplitude should be constant in the absence of absorption, and, therefore, the logarithm of the CT amplitude normalized to its vacuum level should be equal to the integral of the imaginary part of the refractive index along the ray with

a given impact parameter. A similar observation was made by *Jensen et al.* (2003) for the FSI method. (*Gorbunov and Lauritsen*, 2004; *Jensen et al.*, 2004) presented a general analysis, based on the common nature of CT, FSI, and PM methods, and showed that this property is always ensured for the CT/FSI/PM amplitudes by the correct normalization of the amplitude function of the corresponding Fourier Integral Operator (FIO). *Lohmann et al.* (2003a, 2006) presented numerical simulations of the wave optical absorption retrieval based on FSI, for simple spherically-symmetrical models of the atmosphere.

The real atmosphere is not spherically symmetrical, and it contains small-scale turbulence. The effect of the horizontally non-uniform structure on the imaginary refractivity retrieval can be more significant as compared to the real refractivity. *Facheris and Cuccoli* (2003) suggested using the differential method to cancel the effect of the turbulence. Using two channels with adjacent frequencies (for example 17.2 and 17.3 GHz), it was proposed to take the ratio of the two measured amplitudes. Because the frequencies are very close, the two interference patterns due to multipath as well as the amplitude perturbations due to the horizontal gradients of the real refractivity should also be well-correlated. Therefore, taking the logarithmic ratio of the amplitudes should reveal the differential absorption.

The differential approach was developed further by *Gorbunov and Kirchengast* (2005a,b, 2007). They performed numerical modeling of wave propagation in a turbulent atmosphere and showed that the differential approach applied for the measured amplitude is ineffective. Small frequency separation results in the differential absorption being too small and susceptible to measurements noise. With a larger frequency separation, the correlation of the amplitude perturbations in the two channels decreases. *Gorbunov and Kirchengast* (2005a,a, 2007) suggested using the differential approach applied to the CT amplitude. The FIO used in the CT method corrects for most of diffraction and multipath effect. The perturbations due horizontal gradients remain, but they should be well-correlated in all frequency channels, except for very small scales (less than tens of meters). It is no longer required that the frequency separation should be small. Filtering and ratioing the CT amplitudes in different frequency channels effectively reveals the differential absorption. FSI and PM amplitude can be utilized in the same way.

The numerical simulations presented by *Gorbunov and Kirchengast* (2005a,b, 2007) were performed at the level of the transmission retrieval. In this paper we describe an algorithm for the atmospheric profiles retrieval. Our algorithm is based on the integration of the hydrostatic equation, which expresses the vertical gradient of the pressure as a function of the atmospheric profiles (pressure, temperature, and humidity). This equation should

be complemented with the retrieved real and imaginary refractivity profiles. Temperature and humidity can be expressed as functions of pressure, real refractivity and imaginary refractivity at each height level. To solve for temperature and humidity we employ the Rodgers optimization approach (*Rodgers*, 2000) and apply empirical estimates of refractivity retrieval errors. This makes the right part of the hydrostatic equation a known function of pressure and height. After that the hydrostatic equation can be integrated, which gives the pressure, temperature, and humidity profiles.

2 Complex Refractivity Retrieval

In the framework of the CT method, the measured complex wave field $u_j(t)$, where j is the frequency channel number, is transformed by the Fourier Integral Operator (FIO) into the impact parameter representation (details are described by *Gorbunov and Lauritsen* (2004)). The FIO is a linear complex operator with kernel $a(p,t)\exp(ik_jS(p,t))$, where $k_j = 2\pi f_j/c$, f_j is the frequency of the j-th channel, p is the impact parameter, $a(p,t)$ is the amplitude function, and $S(p,t)$ is the phase function. Denote wave field in the transformed space $w_j(p) = A'_j(p)\exp\left(ik_j\Psi'_j(p)\right)$. Bending angles $\epsilon_j(p)$ are algebraic functions of the momenta, $d\Psi'_j(p)/dp$ (*Gorbunov and Lauritsen*, 2004). In particular, in the PM method (*Jensen et al.*, 2004) $\epsilon_j(p) = -d\Psi'_j(p)/dp$. The CT amplitudes in the light zone are equal to $A'_j(p) = A'_{0,j}\exp(-\tau_j(p))K(p)$, where $A_{0,j}$ are the vacuum amplitudes, and $\tau_j(p)$ are transmissions (to be expressed in dB they should be multiplied with $20/\ln 10$), and $K(p)$ is a factor depending from the unknown horizontal gradients of refractivity (*Gorbunov and Kirchengast*, 2005b); $K(p) = 0$ for a spherically symmetric atmosphere. Vacuum amplitudes are found by averaging $A'_j(p)$ over an impact parameter interval where absorption is negligible. Transmissions are retrieved from the CT amplitude:

$$\tau_j(p) = -\ln\frac{A'_j(p)}{A'_{0,j}} + \ln K(p), \tag{1}$$

where unknown term $\ln K(p)$ is the transmission retrieval error (additional focusing/defocusing due to unknown horizontal gradients of refractivity), which is the same for all the frequency channels, except for the small scales (tens of meters) due to diffraction effects (*Gorbunov and Kirchengast*, 2007). On the other hand, transmissions τ_j are equal to the integral of the specific

absorption $\sigma_j(r) = k_j n_j''(r)$ along the ray:

$$\tau_j(p) = 2\int_{r_0}^{\infty} \frac{k_j n_j''(r)}{\sqrt{(n'(r)\,r)^2 - p^2}} n'(r)\,r\,dr, \tag{2}$$

where n' is the real part of the refractivity (it is assumed to be the same for all the frequency channels, because the effects of the dispersion of the real part of the refractive index are negligibly small), n_j'' is the imaginary of refractivity, and $x = n'r$ is the refractive radius.

Using the linear ionospheric correction (*Vorob'ev and Krasil'nikova*, 1994; *Gorbunov*, 2002b), we can derive the neutral atmospheric bending angle profile $\epsilon_N(p)$. Under the assumption of the local spherical symmetry, we can write the standard Abel inversion formulas for the complex refractivity $n_j(x) = n'(x) + in_j''(x)$ (*Kursinski et al.*, 2002):

$$n'(x) = \exp\left(\frac{1}{\pi}\int_x^{\infty} \frac{\epsilon_N(p)\,dp}{\sqrt{p^2 - x^2}}\right), \tag{3}$$

$$n_j''(x) = -\frac{1}{\pi\,k_j}\frac{dx}{dr}\int_x^{\infty} \frac{d\tau_j}{dp}\frac{dp}{\sqrt{p^2 - x^2}}. \tag{4}$$

Because $(d\tau_j/dp)\,dp = (d\tau_j/dp^2)\,dp^2$, the inversion formula for n_j'' can be re-written as a convolution integral over p^2. Factoring out the differentiation from within the convolution, we arrive at another, mathematically equivalent, but numerically more robust inversion formula:

$$n_j''(x(r)) = -\frac{1}{\pi\,k_j\,x(r)}\frac{d}{dr}\int_{x(r)}^{\infty} \frac{\tau_j\,p\,dp}{\sqrt{p^2 - x^2}} \tag{5}$$

Using relation $r = x/n'$, we transform these profiles into functions of altitude $z = r - r_E$, where r_E is the Earth's radius. In presence of horizontal gradients, $n'(z)$ and $n''(z)$ will contain retrieval errors. The retrieval errors consist of the following components: 1) error of n'' due to transmission error $\ln K(p)$, 2) errors of both n' and n'' due to the breach of the assumption of sphericity when applying the Abel inversion (3) and (4), 3) errors due to small scale turbulent structures and measurement noise. The first component of the retrieval error can be canceled by taking differential specific absorption $\Delta\sigma_j(x) = k_j n_j''(x) - k_{j+1} n_{j+1}''(x)$.

3 Atmospheric Profiles Retrieval

The complex refractivity is a function of the atmospheric parameters: pressure, temperature, humidity, liquid water content, rain rate, ice water content, and ozone volume mixing ratio. In this study, we only discuss the retrieval of temperature and humidity. The increase of the number of variables to retrieve makes the problem ill-conditioned if not at the same time the number of adequate channels is increased. We use the Microwave Propagation Model (MPM) (*Liebe*, 1989), which provides the set of equations:

$$n' = N_R^{(MPM)}(P, T, P_w), \tag{6}$$

$$\sigma_j = k_j n_j'' = k_j N_I^{(MPM)}(f_j, P, T, P_w), \tag{7}$$

where $N_R^{(MPM)}$ is the MPM expression for the real part of refractivity, $N_I^{(MPM)}$ is the MPM expression for the imaginary part of refractivity, P is the pressure, T is the temperature, P_w is the water vapor pressure. If we use the differential specific absorption, then we should employ the following equation:

$$\Delta\sigma_j = k_j N_I^{(MPM)}(f_j, P, T, P_w) - k_{j+1} N_I^{(MPM)}(f_{j+1}, P, T, P_w). \tag{8}$$

By solving this nonlinear system of equations, we obtain the atmospheric quantities as a function of the measurements and the pressure, which is treated as a free parameter:

$$T = T(P, n', n''), \tag{9}$$

$$P_w = P_w(P, n', n''), \tag{10}$$

where n'' refers to the complete vector of imaginary refractivities for all the channels.

For solving this system, we use the Rodgers optimization (*Rodgers*, 2000). We will use notation $\mathbf{X}$ for the vector of the unknowns (T, P_w), and $\mathbf{Y}$ for the right part of the system. If the retrieval is based on full specific absorption, then $\mathbf{Y}$ equals $(n', \sigma_1, ...\sigma_N)$, where N is the number of channels. If the retrieval is based on the differential specific absorption, then $\mathbf{Y}$ equals $(n', \Delta\sigma_1, ..., \Delta\sigma_{N-1})$. The system can be symbolically written in the following form:

$$\mathbf{Y} = \mathbf{Y}^{MPM}(\mathbf{X}) \tag{11}$$

The system is solved iteratively. By specifying the initial approximation $\mathbf{X}_0$, a priori inverse covariance matrix $\hat{\mathbf{C}}$ of the vector of unknowns $\mathbf{X}$, a posteriori inverse covariance matrix of the errors of the right part $\hat{\mathbf{W}}$, the matrix of the linearized system

$$\hat{\mathbf{K}} = \frac{\partial \mathbf{Y}^{MPM}}{\partial \mathbf{X}}, \tag{12}$$

each next iteration can be expressed as follows:

$$\mathbf{X}_{i+1} = \mathbf{X}_i + \left(\hat{\mathbf{K}}^T\hat{\mathbf{W}}\hat{\mathbf{K}} + \hat{\mathbf{C}}\right)^{-1}\hat{\mathbf{K}}^T\hat{\mathbf{W}}\left(\mathbf{Y} - \mathbf{Y}^{MPM}\left(\mathbf{X}_i\right)\right). \quad (13)$$

The iterations stop, when the increment of $\mathbf{X}$ becomes smaller than some pre-defined tolerance limit.

The solution of this system is substituted into the hydrostatic equation:

$$\frac{d\ln P\left(z\right)}{dz} = \frac{g\left(z\right)}{R_d\left(T\left(P\left(z\right), n'\left(z\right), n''\left(z\right)\right) + c_q q\left(P\left(z\right), n'\left(z\right), n''\left(z\right)\right)\right)}, \quad (14)$$

where q is the specific humidity, $c_q = \frac{R_v}{R_d} - 1$, R_d is the gas constant for the dry air, R_v is the gas constant for the water vapor. The specific humidity can be expressed as a function of the pressure and water vapor pressure:

$$q = \frac{a_q P_w}{P - \left(1 - a_q\right)P_w}, \quad (15)$$

where $a_q = R_d/R_v$. Given retrieved refractivities $n'\left(z\right), n''\left(z\right)$, the right part is function of $P\left(z\right)$, and this equation can be integrated producing the atmospheric profiles $P\left(z\right)$, $T(z) = T\left(P\left(z\right), n'\left(z\right), n''\left(z\right)\right)$, and $q\left(z\right) = q\left(P\left(z\right), n'\left(z\right), n''\left(z\right)\right)$.

4 Numerical Implementation

Our numerical implementation of the Complex Refractivity Inversion (CRI) uses the downward integration of equation (14) by the Runge–Kutta method. The integration starts at a large height of 120 km. Above 15 km, we integrate the equation for the dry atmosphere, assuming $P_w = 0$ and

$$n' = 1 + C\frac{P}{T}, \quad (16)$$

$$T\left(P, n'\right) = \frac{CP}{n' - 1}, \quad (17)$$

where $C = 77.6\times10^{-6}$ K/mb. The use of dry inversion above 15 km allows for the reduction of the CPU time usage required for a relatively slow iterative Rodgers optimization. The resulting temperature at 15 km is used for the computation of the initial condition for the complex refractivity inversion, which starts here.

The a posteriori error covariance matrix of the right part $\hat{\mathbf{W}}^{-1}$ is taken in the diagonal form. The diagonal element corresponding to the real refractivity is estimated using the statistical optimization as described in (*Gorbunov*,

2002b). The errors of retrieved specific absorption for each channel are estimated as follows:

$$\delta\sigma_j = \frac{\alpha}{k_j}\left(\frac{A'_{0,j}}{A'_j(p)}\right)^{\beta}, \tag{18}$$

where $\alpha = 1$ N-unit and $\beta = 2$ are empirical coefficients. This formula expresses the fact that the retrieval errors increase with decreasing amplitude of the signal.

Below 15 km, after each step of the numerical integration of the hydrostatic equation, we specify the following initial approximation for the next step:

$$\mathbf{X}_0(z_i) = (T_0(z_i), q_0(z_i)) \tag{19}$$

$$T_0(z_i) = T_0(z_{i-1}) + (z_i - z_{i-1})\frac{dT_{MSIS}(z)}{dz}, \tag{20}$$

$$q_0(z_i) = q_0(z_{i-1}), \tag{21}$$

where $T_{MSIS}(z)$ is the MSIS temperature profile. The a priori error covariance matrix $\hat{\mathbf{C}}$ of the vector of unknowns $\mathbf{X}$ is taken in the diagonal form. The error of the temperature is assumed to be $\gamma\Delta z$, where $\gamma = 2$ K/km is the empirical constraint of the temperature gradient. The error of the water vapor pressure was taken to be 1 hPa.

We avoid using the first guess from an NWP model as the initial approximation, because we are developing a stand-alone retrieval algorithm. The retrieval results should not contain any a priori information if targeted use includes allowance for data assimilation into an NWP model. This avoids that the first guess might be used twice: in the inversion and in the assimilation.

5 Numerical simulations

In our numerical simulation we model occultations with 3 frequency channels: 9.7, 17.25, and 22.6 GHz. To model the atmosphere, we employ global gridded fields of thermodynamic state variables from operational analyses of the European Centre for Medium-Range Weather Forecasts (ECMWF). Using the phase screens (*Martin*, 1992) and Fourier Integral Operators (*Gorbunov and Lauritsen*, 2004) techniques, we simulate the wave propagation between a space-borne transmitter and receiver. This produces artificial multi-channel measurements of the phase and the amplitude, which are then used as the input data for the retrieval chain. The retrieved variables are then compared with reference ones from the original ECMWF fields.

Figures 1, 2, 3, 4, and 5 show the simulation results for the first example. Here we model an atmosphere without horizontal gradients, i.e., we only use

vertical profiles of ECMWF variables from the given location. Because the errors due to eventual horizontal gradients were excluded here, we were using the inversion of full specific absorption.

Figure 1 presents the retrieved CT-amplitudes, which are now equal to $A'_{0,j} \exp(-\tau_j(p))$. The absorption in channel 3 (22.6 GHz), which is located near the maximum of the water vapor absorption line, is strong enough for the signal to disappear below the 6 km impact height. Therefore, below 6 km the error estimate (18) for this channel will increase and suppress its use in the inversion.

Figure 2 presents the retrieved specific absorption profiles. The profile for channel 3 below 6 km indicates large errors, due to increasingly weak signal. Figures 3 and 4 presents the retrieved specific humidity and temperature, respectively. Humidity and temperature were retrieved using the complex refractivity inversion algorithm described above in Sections 3 and 4. Figure 5 presents the specific absorption for the three channels, evaluated from the retrieved temperature and humidity. Due to the use of error estimate and temperature gradient constraint, they agree better with the reference values, as compared to the retrieved absorption profiles.

The retrieved humidity and temperature are, therefore, well consistent with the reference complex refractivity. Still, relatively small errors of humidity (not exceeding 0.6 g/kg below 3 km) correspond to temperature errors reaching 3 K, which are too large. This indicates a need for a stronger constraint of temperature gradient.

Figures 6 through 20 present three further examples with the same simulation setup: 3 X/K frequency channels and a spherically-symmetric atmosphere. They corroborate the conclusions made from the first example.

Figures 21 through 25 present a numerical simulation with horizontal gradients. The location and observation geometry are the same as in the previous five Figures. The inversion uses differential specific absorption.

Figure 21 presents the retrieved CT-amplitudes, which now include the unknown factor of $K(p)$ resulting from horizontal gradients. This factor is visible when comparing this Figure with Figure 16. Figure 22 presents the reference and retrieved differential attenuation, which are in a good agreement. However, the retrieved differential specific absorption notably differs from the reference one, which indicates the Abel inversion errors due to horizontal gradients, as discussed above in Section 3. Figures 24 and 25 present the retrieved humidity and temperature compared to the reference ones. The Abel inversion error of humidity is clearly visible. The temperature retrieval does not significantly differ from the previous example without horizontal gradients.

6 Conclusion

In this report we described the first implementation of the complex refractivity inversion algorithm. The algorithm is a first step to the development of the system of processing data from anticipated future LEO–LEO missions. The algorithm is based on the downward integration of the hydrostatic equation, where the temperature and humidity are expressed as functions of the pressure, which is the independent integration variable, and of retrieved complex refractivity. At each integration step, we solve for temperature and humidity. The equations are derived from the Liebe microwave propagation model, which supplies complex refractivity as a function of thermodynamic state variables. The system of equations is solved by the iterative Rodgers optimization. To this end, at each iteration the system of equations is linearized and solved by quasi-inversion of its matrix in the framework of the statistical optimization employing the a posteriori error estimates of the retrieved complex refractivity, a priori error estimates of the unknown temperature and humidity, and an additional constraint of the temperature gradient.

To validate the algorithm we performed numerical simulations. We used gridded fields of thermodynamic state variables from ECMWF operational forecasts. Using multiple phase screens and Fourier Integral Operators techniques, we simulated radio occultation experiments and created artificial measurement data sets. The artificial were pre-processed using the CT method to derive bending angles and transmission. From the bending angles and transmissions we then derived the complex refractivity using the Abel integral inversion. The complex refractivity obtained was used as the input data for our algorithm of the atmospheric state retrieval. The numerical simulation design included three frequency channels: 9.7, 17.25, and 22.6 GHz, located at the wing of the water vapor absorption line.

We performed a series of numerical simulations with a spherically symmetric atmosphere, in order to exclude errors resulting from horizontal gradients. It was shown that under these conditions it is possible to retrieve humidity with an accuracy of about 0.5 g/kg in the lowest about 3 km. However, this humidity error corresponds to a temperature error of about 3 K. This indicates the need for stronger physical constraints for the temperature gradient, which may allow for stabilizing the temperature retrieval.

We also performed 3D numerical simulations accounting for horizontal gradients. In our runs, the retrieval error of the Abel inversion was mostly visible in the humidity retrieval, while the quality of the temperature inversion was not significantly influenced. This is explained by the implementation of temperature gradient constraint.

In this report we did not discuss the sensitivity of retrievals to noise. The

investigation of the stability of the algorithm with respect to turbulent fluctuations and measurement noise and determination of the optimal filtering parameters and corresponding a priori and a posteriori error estimates are the subject of further investigations.

Acknowledgement 1 *The authors gratefully acknowledge J. Fritzer, M. Schwärz, and Andreas Gobiet (Wegener Center, Univ. of Graz, Austria) for discussions and software assistance during the numerical simulations. The work was supported by the Russian Foundation for Basic Research, grant 06-05-64359. The work was funded by the ESA Prodex Arrangement No. 90152-CN1 (Project Advanced Topics in RO Modelling and Retrieval).*

References

Engeln, A. V., G. Nedoluha, G. Kirchengast, and S. Bühler, One-dimensional variational (1-D Var) retrieval of temperature, water vapor, and a reference pressure from radio occultation measurements: A sensitivity analysis, *J. Geophys. Res.*, *108*, 4337, doi: 10.1029/2002JD002,908, 2003.

Eyre, J. R., Assimilation of radio occultation measurements into a numerical weather prediction system, *Technical Memorandum No. 199*, European Center for Medium-Range Weather Forecast, 1994.

Facheris, L., and F. Cuccoli, Analysis of differential spectral attenuation measurements applied to a LEO-LEO link, *ESA-ACEPASS Report (contract 16743/02/NL/FF)*, Inst. of Elect. and Telecommunications, Univ. of Florence, 2003.

Gorbunov, M. E., Canonical transform method for processing GPS radio occultation data in lower troposphere, *Radio Sci.*, *37*, 9–1–9–10, doi:10.1029/2000RS002,592, 2002a.

Gorbunov, M. E., Ionospheric correction and statistical optimization of radio occultation data, *Radio Sci.*, *37*, 17–1–17–9, doi: 10.1029/2000RS002,370, 2002b.

Gorbunov, M. E., and G. Kirchengast, Advanced wave-optics processing of LEO-LEO radio occultation data in presence of turbulence, *Tech. Report for ESA/ESTEC No. 1/2005*, University of Graz, Austria, 2005a.

Gorbunov, M. E., and G. Kirchengast, Processing X/K band radio occultation data in the presence of turbulence, *Radio Science*, *40*, RS6001, doi: 10.1029/2005RS003,263, 2005b.

Gorbunov, M. E., and G. Kirchengast, Fluctuations of radio occultation signals in X/K band in the presence of anisotropic turbulence and differential transmission retrieval performance, *Radio Science*, *42*, RS4025, doi: 10.1029/2006RS003,544, 2007.

Gorbunov, M. E., and L. Kornblueh, Principles of variational assimilation of GNSS radio occultation data, *Report No. 350*, Max Planck Institute for Meteorology, Hamburg, 2003.

Gorbunov, M. E., and K. B. Lauritsen, Analysis of wave fields by Fourier Integral Operators and its application for radio occultations, *Radio Sci.*, *39*, RS4010, doi:10.1029/2003RS002,971, 2004.

Healy, S. B., J. R. Eyre, M. Hamrud, and J.-N. Thepaut, Assimilating GPS radio occultation measurements with two-dimensional bending angle observation operators, *Q. J. R. Meteorol. Soc.*, *133*, 12131227, 2007.

Jensen, A. S., M. S. Lohmann, H.-H. Benzon, and A. S. Nielsen, Full spectrum inversion of radio occultation signals, *Radio Sci.*, *38*, 6–1–6–15, doi: 10.1029/2002RS002,763, 2003.

Jensen, A. S., M. S. Lohmann, A. S. Nielsen, and H.-H. Benzon, Geometrical optics phase matching of radio occultation signals, *Radio Sci.*, *39*, RS3009, doi: 10.1029/2003RS002,899, 2004.

Kirchengast, G., and P. Høeg, The ACE+ mission: Atmosphere and climate explorer based on GNSS-LEO and LEO-LEO radio occultation, in *Occultations for Probing Atmosphere and Climate*, edited by G. Kirchengast, U. Foelsche, and A. K. Steiner, pp. 201–220, Springer, Berlin - Heidelberg, 2004.

Kirchengast, G., J. Fritzer, M. Schwaerz, S. Schweitzer, and L. Kornblueh, The atmosphere and climate explorer mission ACE+: Scientific algorithms and performance overview, *Tech. Report for ESA/ESTEC No. 2/2004*, Inst. for Geophys., Astrophys., and Meteorol., Univ. of Graz, Austria, 2004.

Kursinski, E. R., S. Syndergaard, D. Flittner, D. Feng, G. Hajj, B. Herman, D. Ward, and T. Yunck., A microwave occultation observing system optimized to characterize atmospheric water, temperature and geopotential via absorption, *Journal of Atmospheric and Oceanic Technology*, *19*, 1897–1914, 2002.

Liebe, H. J., MPM - an atmospheric millimeter wave propagation model, *Int. J. Infrared and Millimeter Waves*, *10*, 631–650, 1989.

Liu, H., and X. Zou, Improvements to a GPS radio occultation ray-tracing model and their impacts on assimilation of bending angle, *J. Geophys. Res.*, *108*, 4548, doi: 10.1029/2002JD003,160, 2003.

Lohmann, M. S., A. S. Jensen, H.-H. Benzon, and A. S. Nielsen, Radio occultation retrieval of atmospheric absorption based on FSI, *Scientific Report 03-20*, Danish Meteorological Institute, Copenhagen, 2003a.

Lohmann, M. S., L. Olsen, H.-H. Benzon, A. S. Nielsen, A. S. Jensen, and P. Høeg, Water vapour profiling using LEO-LEO inter-satellite links, in

Proceedings of the Symposium "Atmospheric Remote Sensing Using Satellite Navigation Systems", URSI section F/G, Matera, Italy, 2003b.

Lohmann, M. S., A. S. Jensen, H.-H. Benzon, and A. S. Nielsen, Application of window functions for full spectrum inversion of cross-link radio occultation data, *Radio Sci.*, *41*, RS3001, doi:10.1029/2005RS003,273, 2006.

Martin, J., Simulation of wave propagation in random media: theory and applications, in *Wave propagation in random media (scintillations)*, edited by V. I. Tatarskii, A. Ishimaru, and V. U. Zavorotny, pp. 463–486, SPIE - The International Society for Optical Engineering and Institute of Physics Publishing, Bellingham, Washington USA, Bristol and Philadelphia, 1992.

Rodgers, C., *Inverse Methods for Atmospheric Sounding - Theory and Practice*, World Scientific Publishing, Signapore, 2000.

Vorob'ev, V. V., and T. G. Krasil'nikova, Estimation of the accuracy of the atmospheric refractive index recovery from Doppler shift measurements at frequencies used in the NAVSTAR system, *Izvestiya Academy of Sciences SSSR, Atmospheric and Oceanic Physics, English Translation*, *29*, 602–609, 1994.

Zou, X., F. Vandenberghe, B. Wang, M. E. Gorbunov, Y.-H. Kuo, S. Sokolovskiy, J. C. Chang, J. G. Sela, and R. Anthes, A ray-tracing operator and its adjoint for the use of GPS/MET refraction angle measurements, *Journal of Geophysical Research - Atmospheres*, *104*, 22,301–22,318, 1999.

Figures

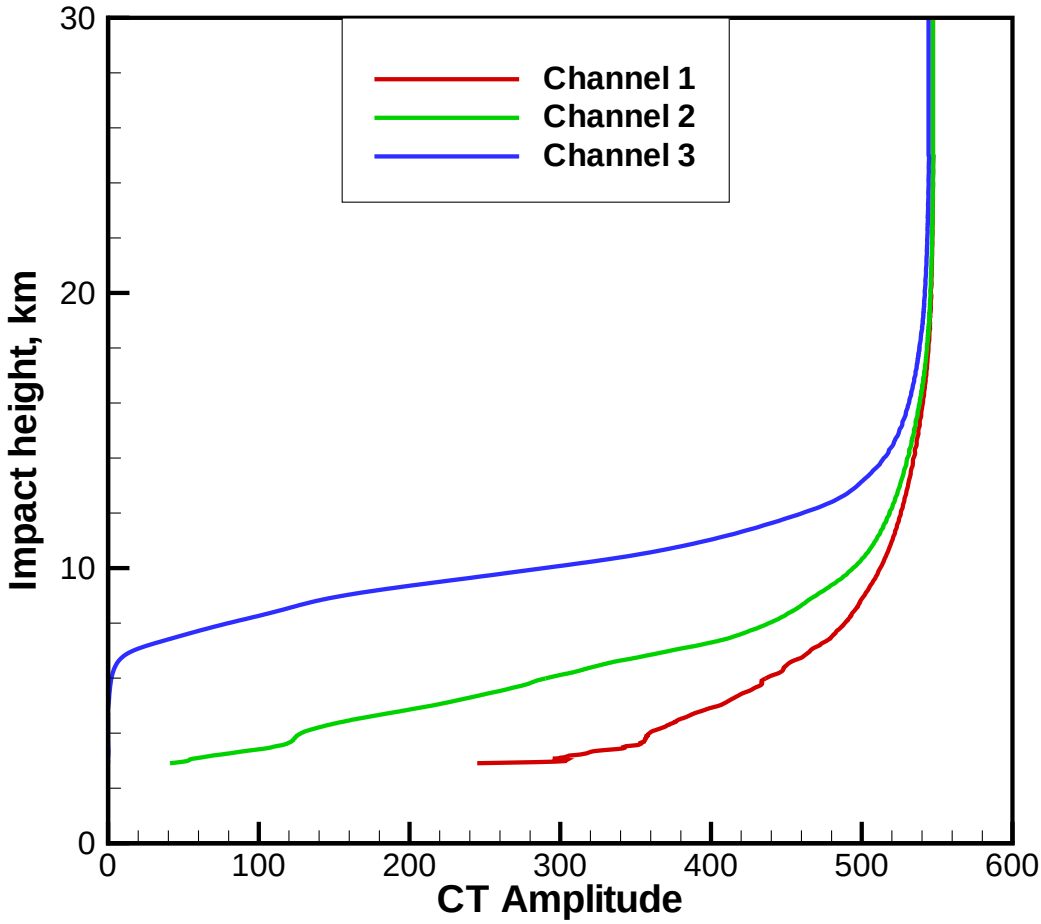

Figure 1: Simulated occultation event at UTC 00:00, September 06, 2007, 10.08°N 59.99°E. CT amplitudes for 9.7, 17.25, and 22.6 GHz.

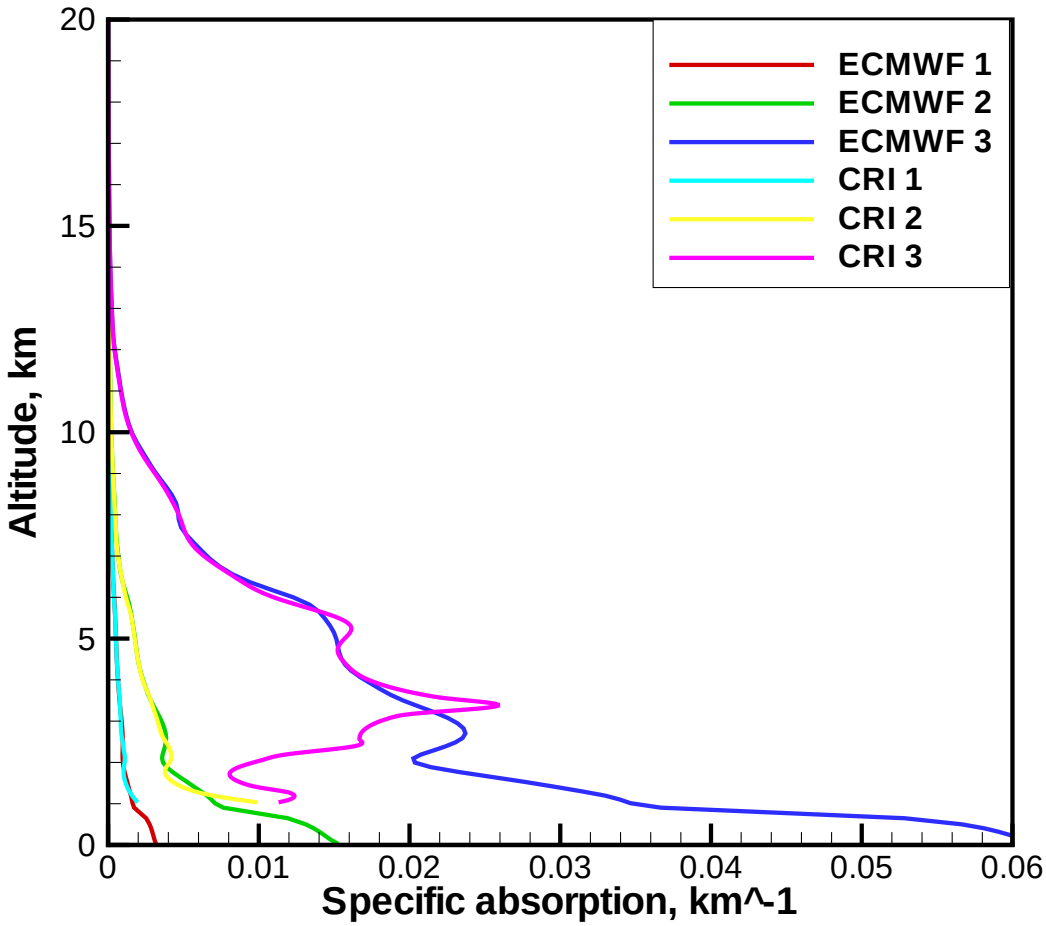

Figure 2: Simulated occultation event at UTC 00:00, September 06, 2007, 10.08°N 59.99°E. Retrieved (CRI) and reference (ECMWF) specific absorption for 9.7, 17.25, and 22.6 GHz.

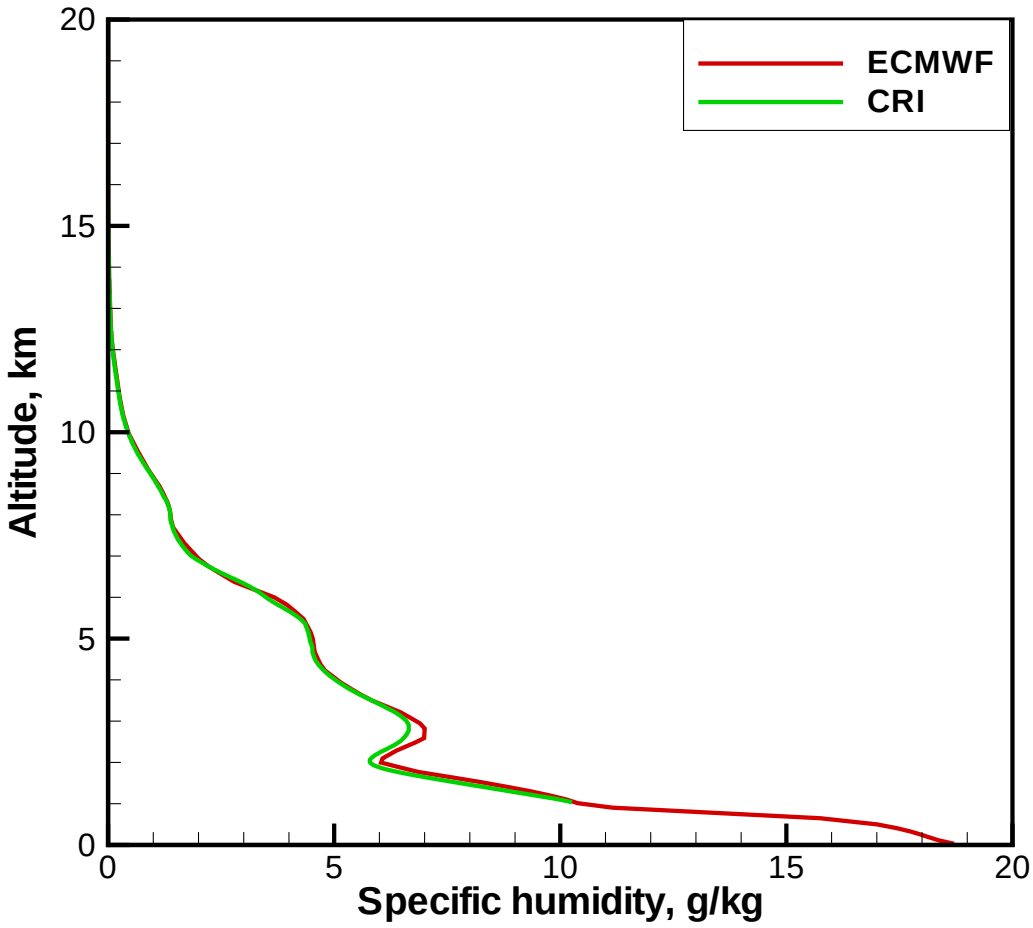

Figure 3: Simulated occultation event at UTC 00:00, September 06, 2007, 10.08°N 59.99°E. Retrieved (CRI) and reference (ECMWF) specific humidity for 9.7, 17.25, and 22.6 GHz.

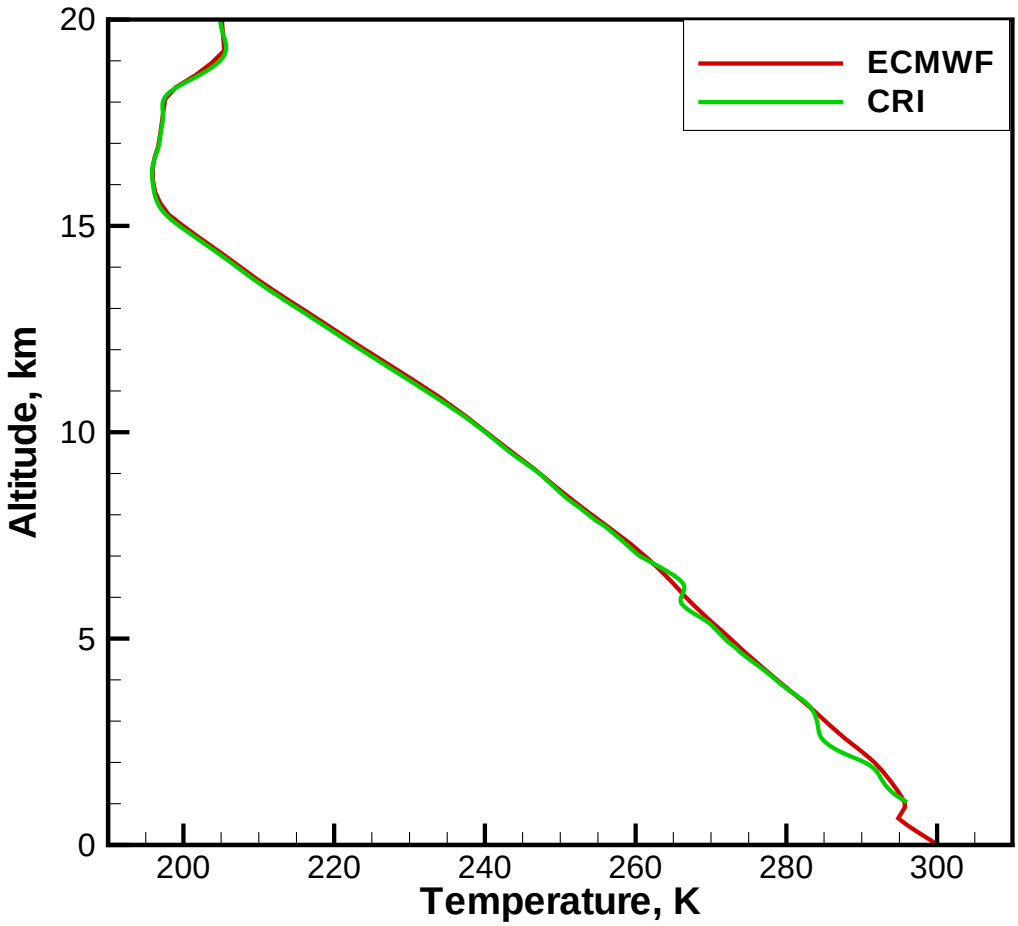

Figure 4: Simulated occultation event at UTC 00:00, September 06, 2007, 10.08°N 59.99°E. Retrieved (CRI) and reference (ECMWF) temperature for 9.7, 17.25, and 22.6 GHz.

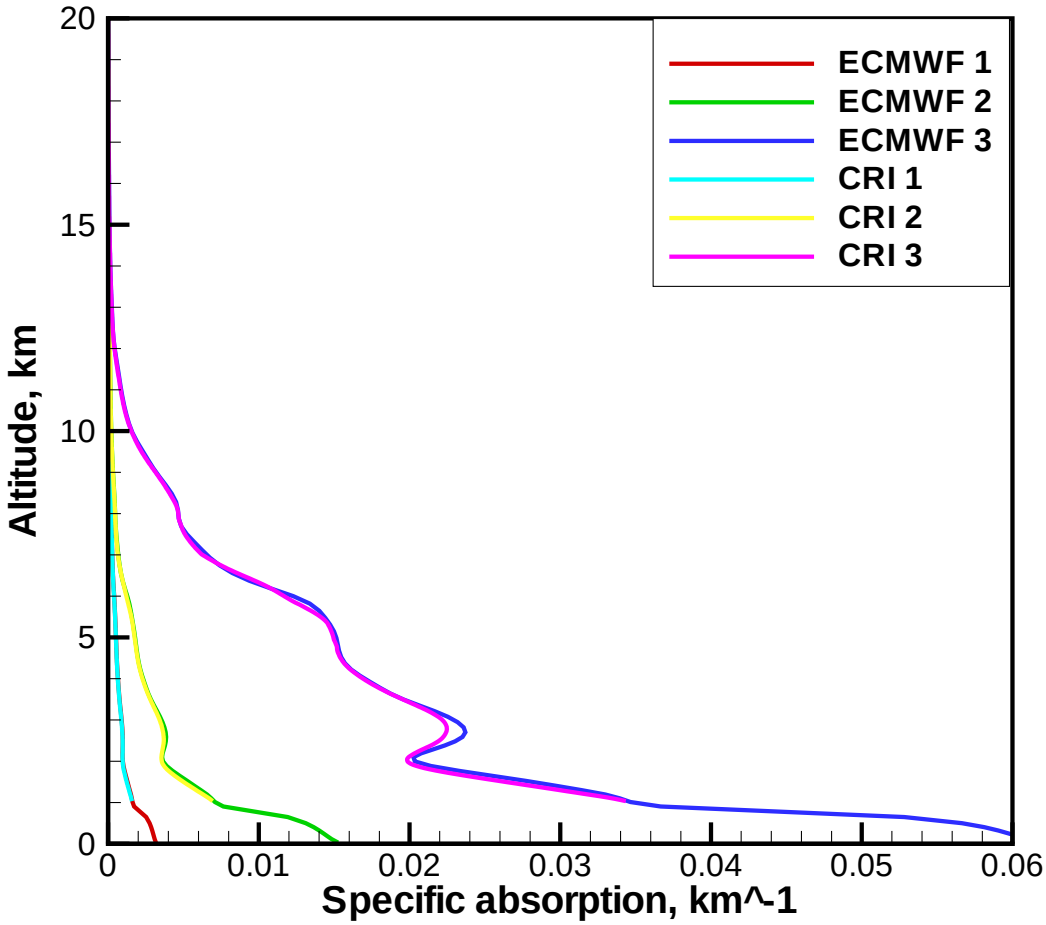

Figure 5: Simulated occultation event at UTC 00:00, September 06, 2007, 10.08°N 59.99°E. Specific absorption computed from retrieved temperature and humidity (CRI) and reference specific (ECMWF) for 9.7, 17.25, and 22.6 GHz.

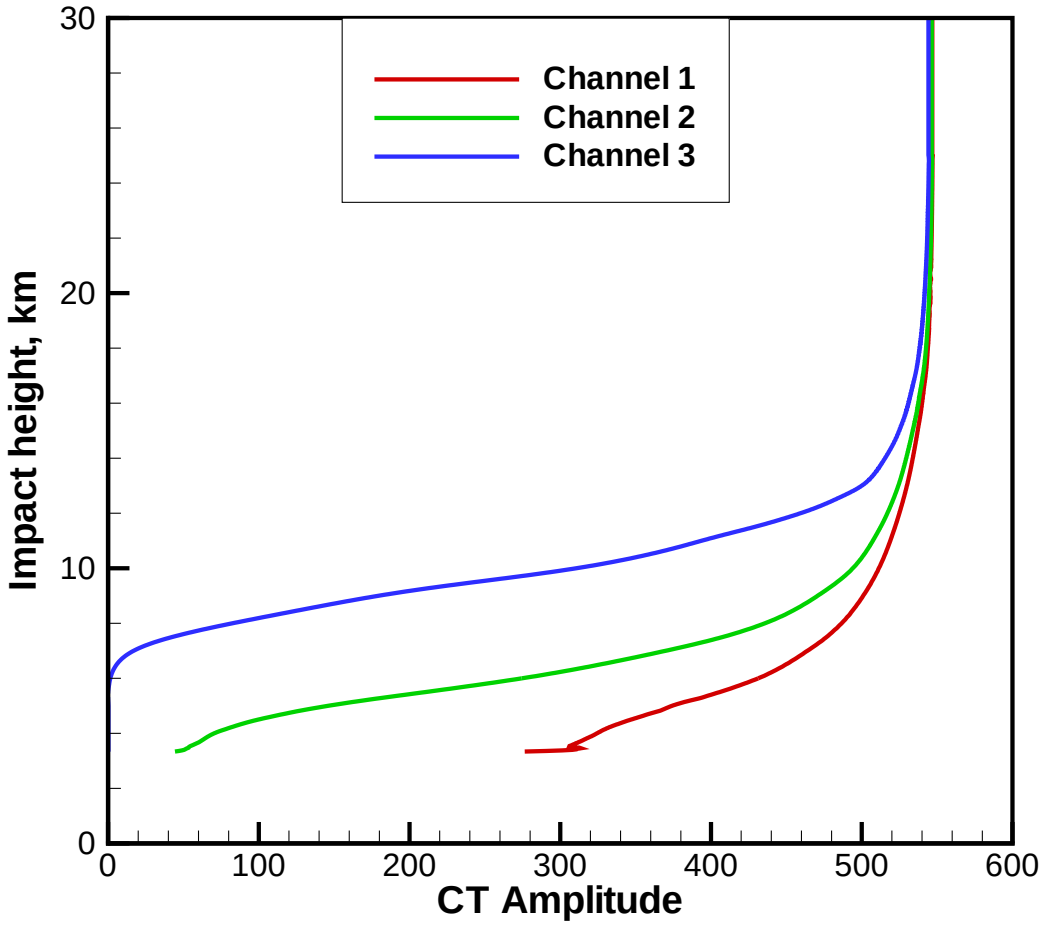

Figure 6: Simulated occultation event at UTC 00:00, September 06, 2007, 10.08°N 19.99°E. CT amplitudes for 9.7, 17.25, and 22.6 GHz.

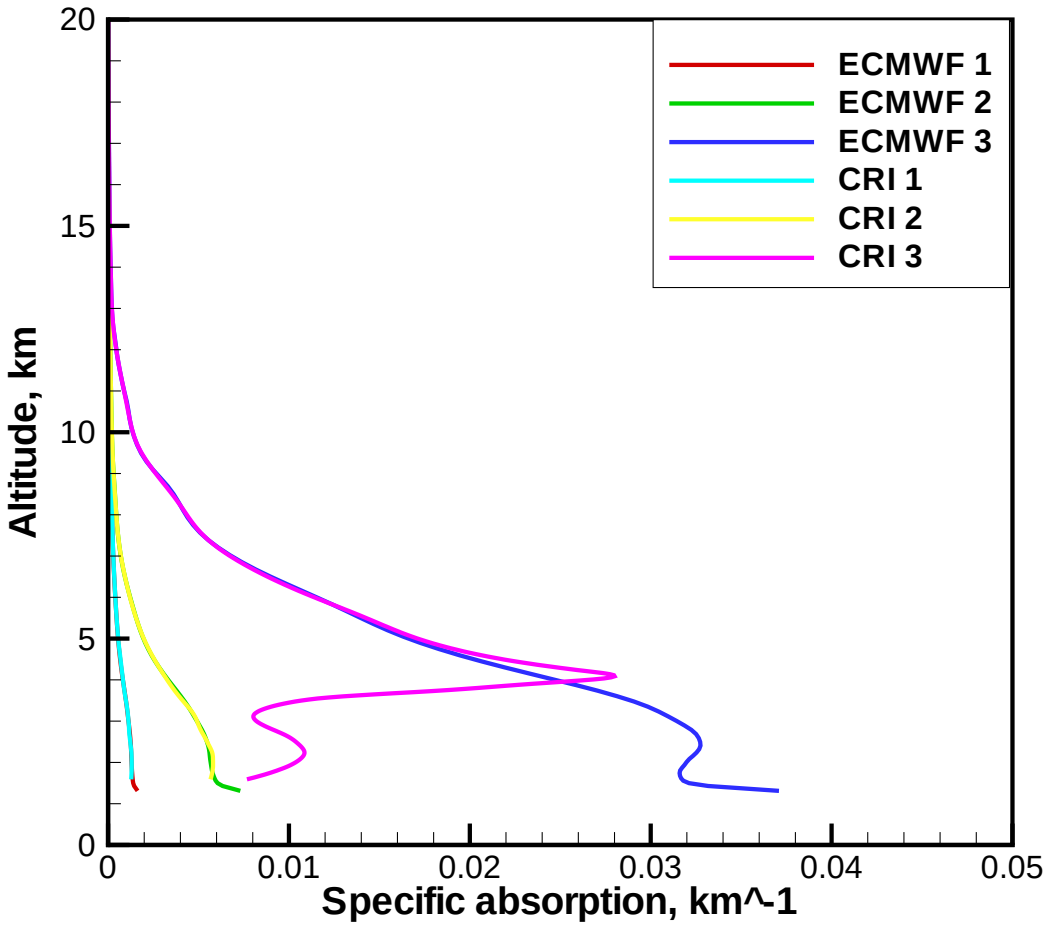

Figure 7: Simulated occultation event at UTC 00:00, September 06, 2007, 10.08°N 39.99°E. Retrieved (CRI) and reference (ECMWF) specific absorption for 9.7, 17.25, and 22.6 GHz.

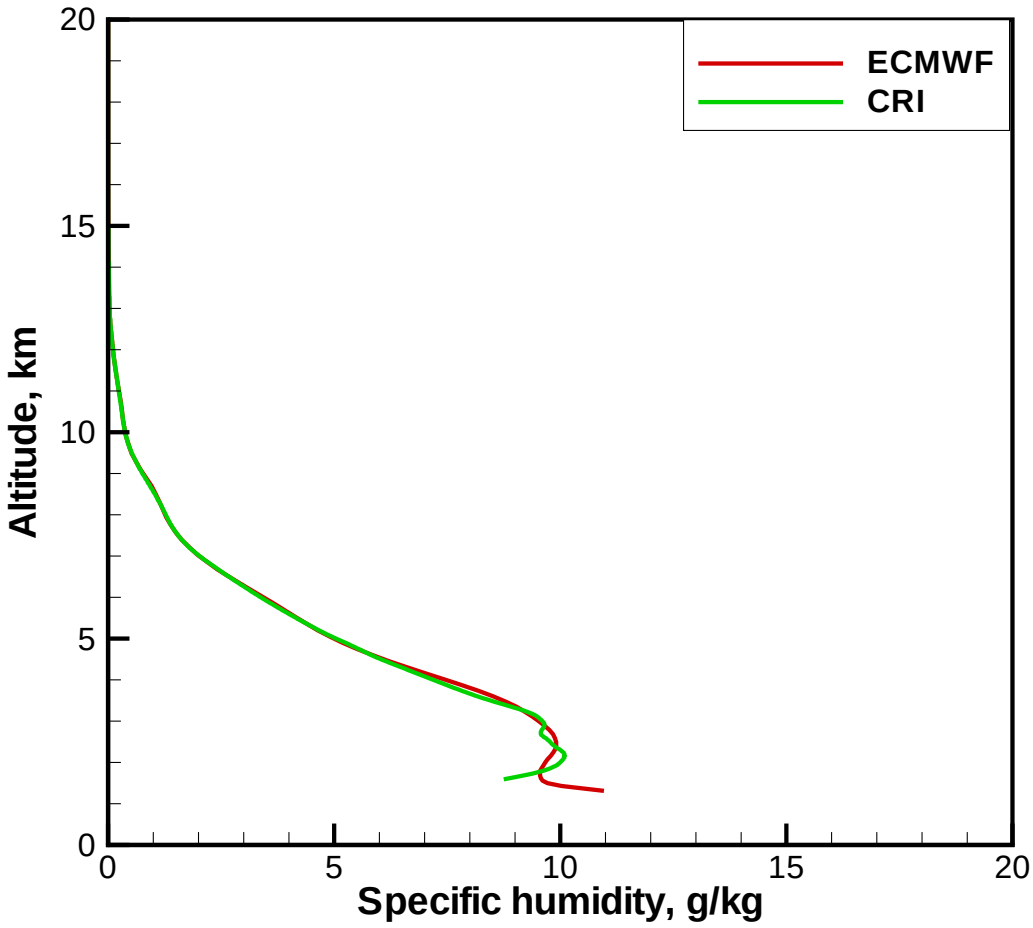

Figure 8: Simulated occultation event at UTC 00:00, September 06, 2007, 10.08°N 39.99°E. Retrieved (CRI) and reference (ECMWF) specific humidity for 9.7, 17.25, and 22.6 GHz.

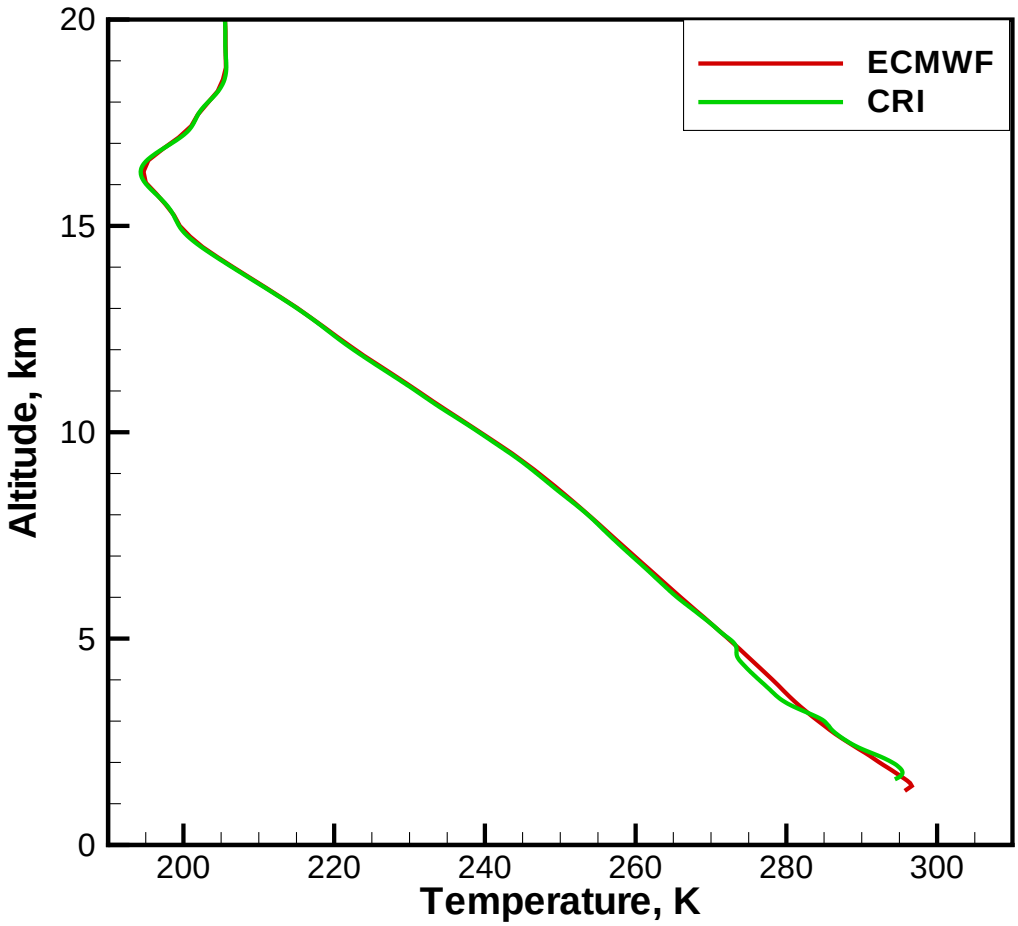

Figure 9: Simulated occultation event at UTC 00:00, September 06, 2007, 10.08°N 39.99°E. Retrieved (CRI) and reference (ECMWF) temperature for 9.7, 17.25, and 22.6 GHz.

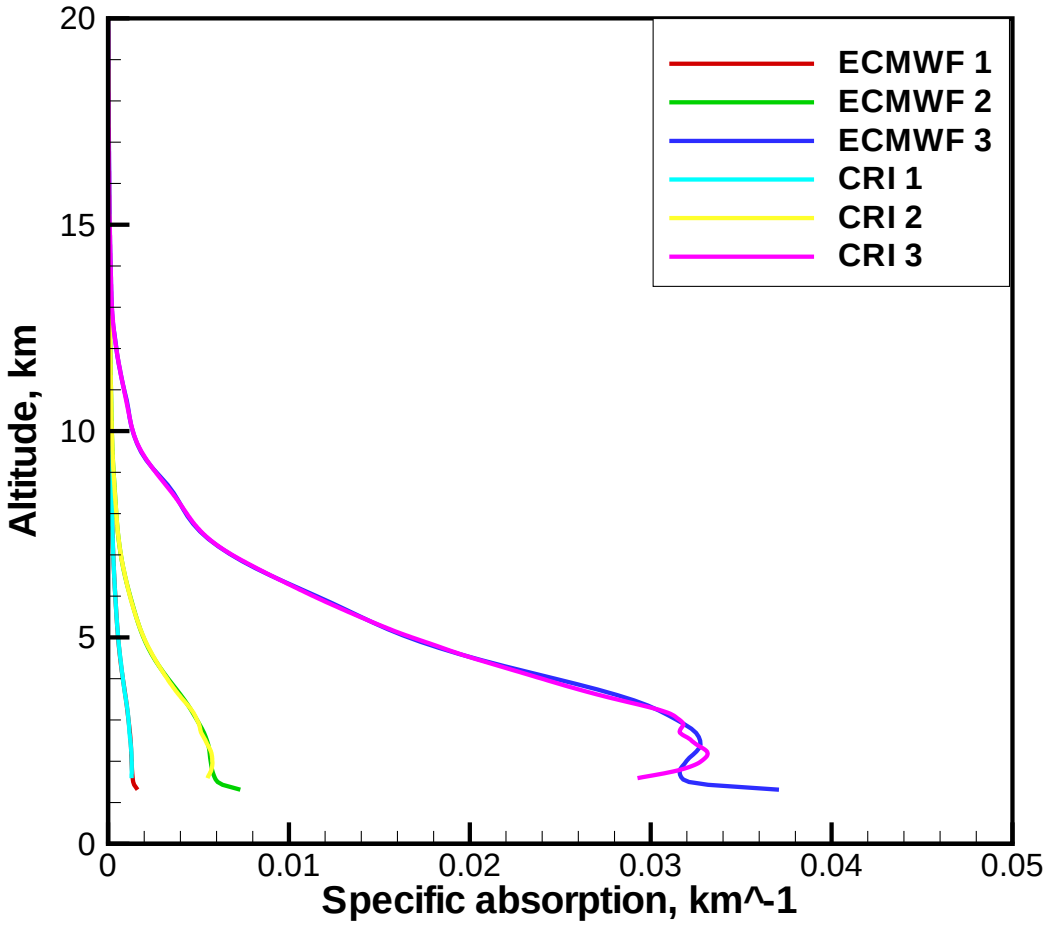

Figure 10: Simulated occultation event at UTC 00:00, September 06, 2007, 10.08°N 39.99°E. Specific absorption computed from retrieved temperature and humidity (CRI) and reference specific (ECMWF) for 9.7, 17.25, and 22.6 GHz.

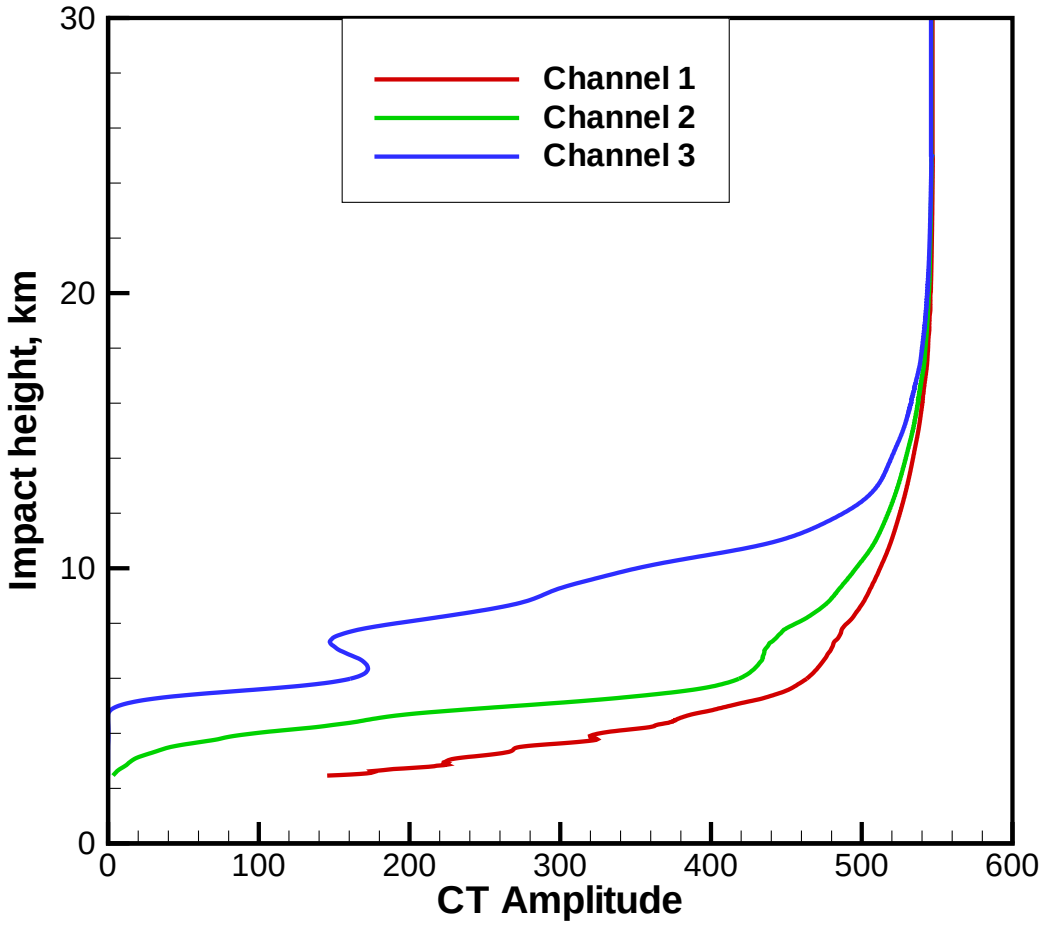

Figure 11: Simulated occultation event at UTC 00:00, September 06, 2007, 10.06°S 49.99°E. CT amplitudes for 9.7, 17.25, and 22.6 GHz.

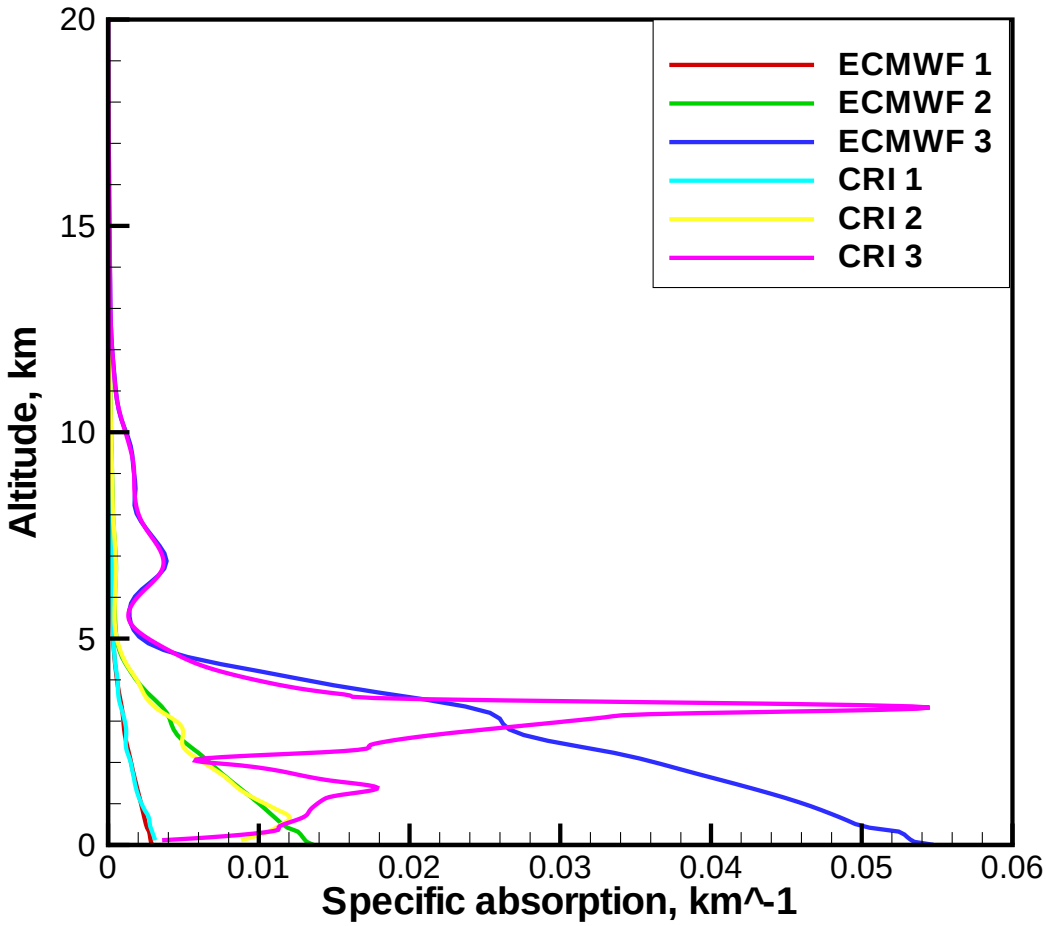

Figure 12: Simulated occultation event at UTC 00:00, September 06, 2007, 10.06°S 49.99°E. Retrieved (CRI) and reference (ECMWF) specific absorption for 9.7, 17.25, and 22.6 GHz.

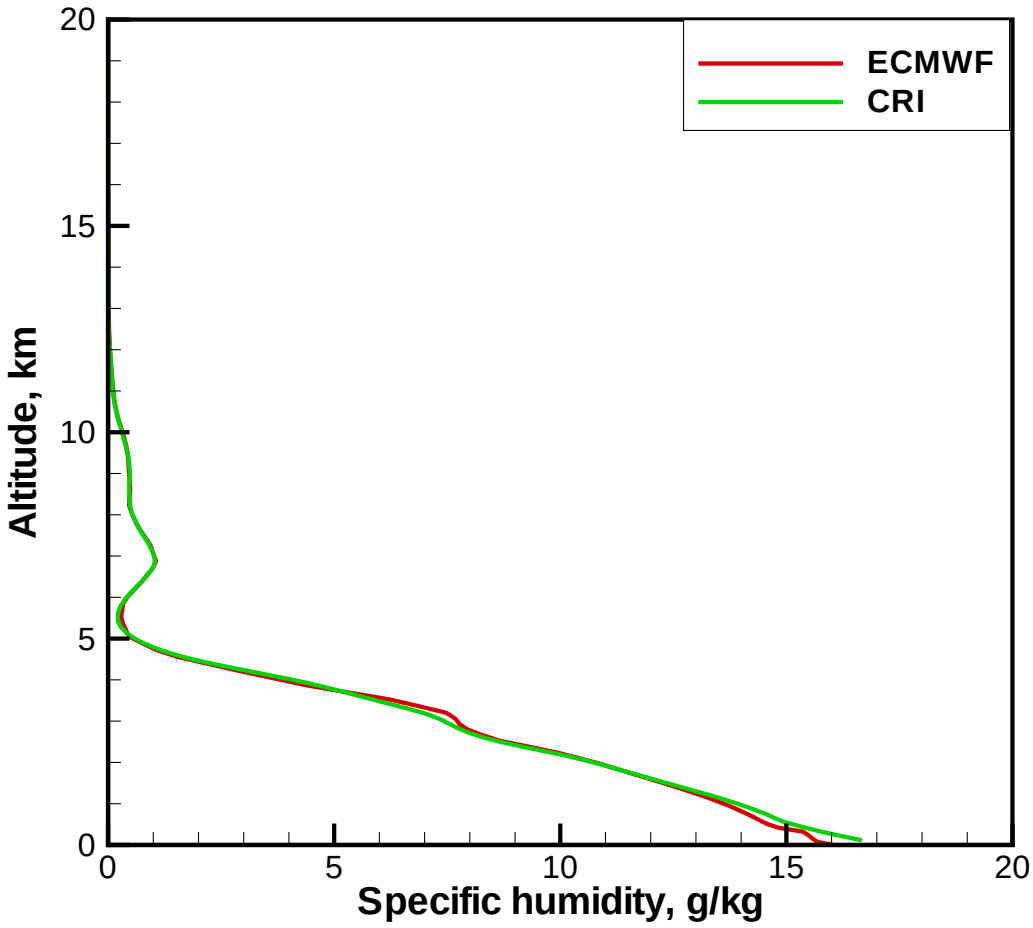

Figure 13: Simulated occultation event at UTC 00:00, September 06, 2007, 10.06°S 49.99°E. Retrieved (CRI) and reference (ECMWF) specific humidity for 9.7, 17.25, and 22.6 GHz.

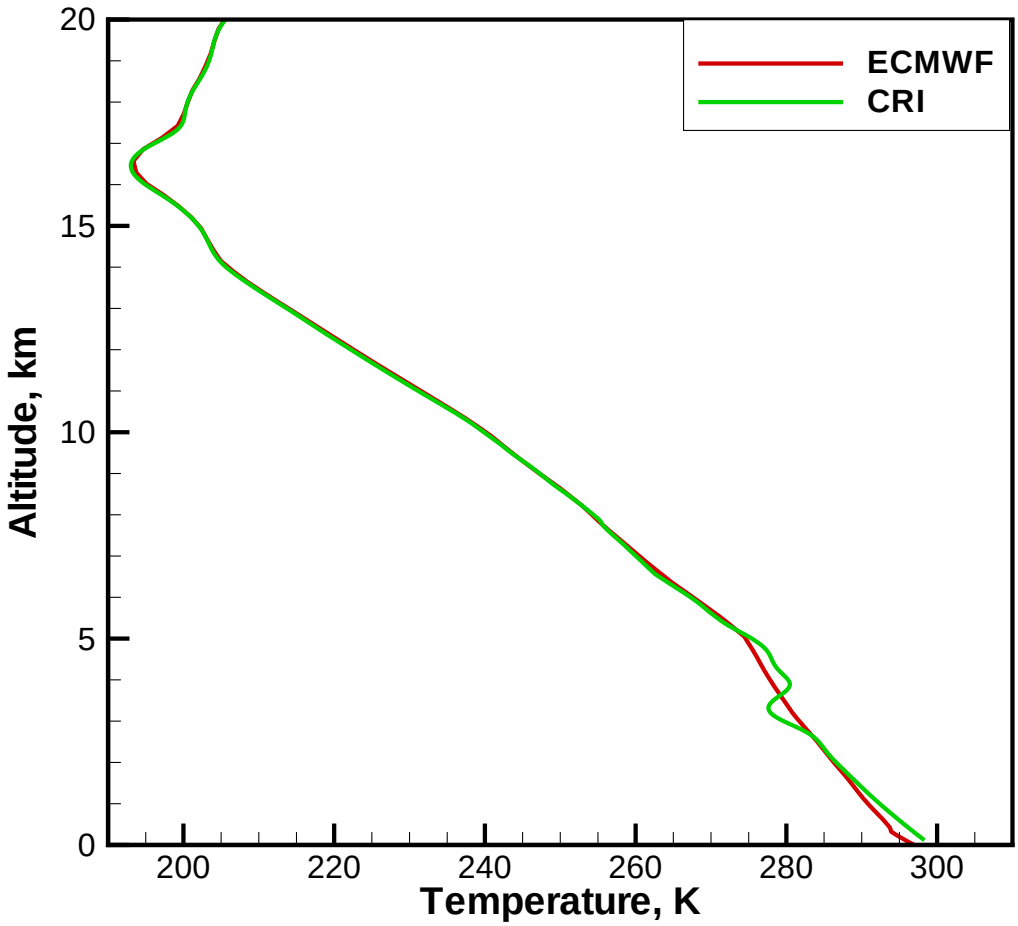

Figure 14: Simulated occultation event at UTC 00:00, September 06, 2007, 10.06°S 49.99°E. Retrieved (CRI) and reference (ECMWF) temperature for 9.7, 17.25, and 22.6 GHz.

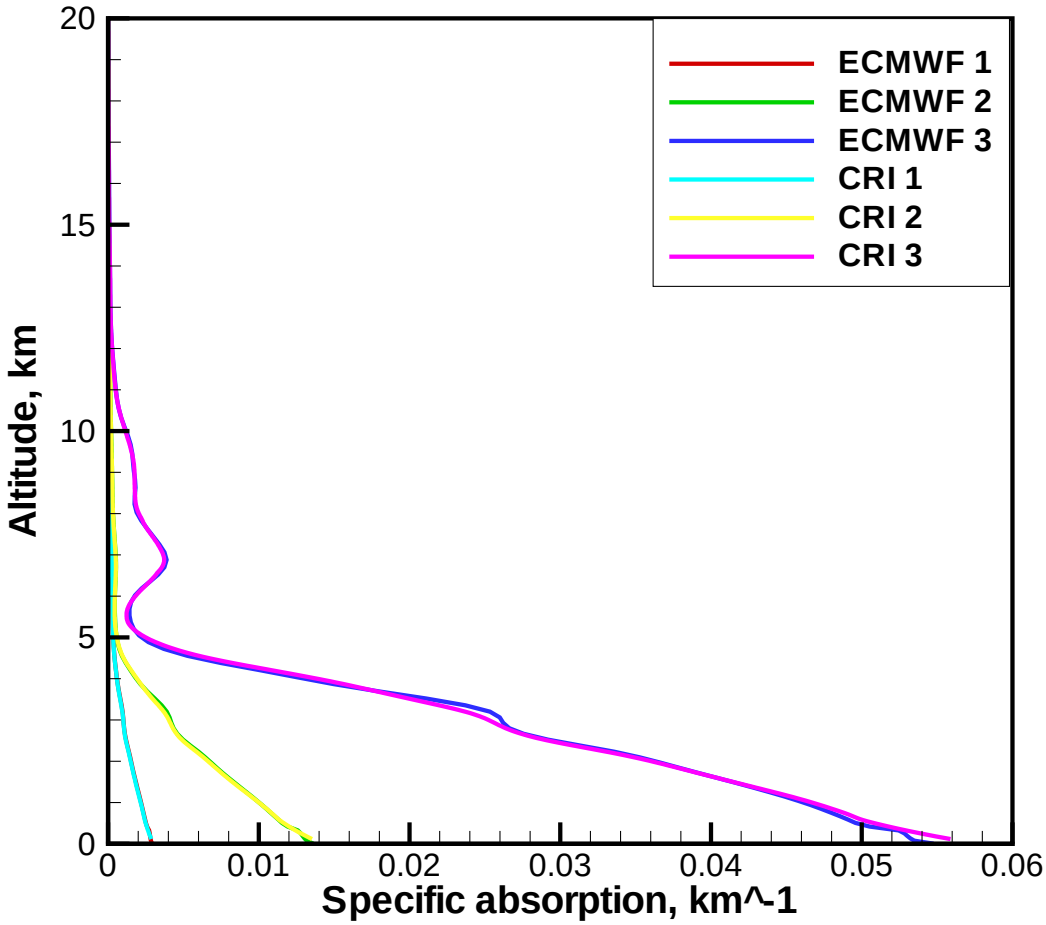

Figure 15: Simulated occultation event at UTC 00:00, September 06, 2007, 10.06°S 49.99°E. Specific absorption computed from retrieved temperature and humidity (CRI) and reference specific (ECMWF) for 9.7, 17.25, and 22.6 GHz.

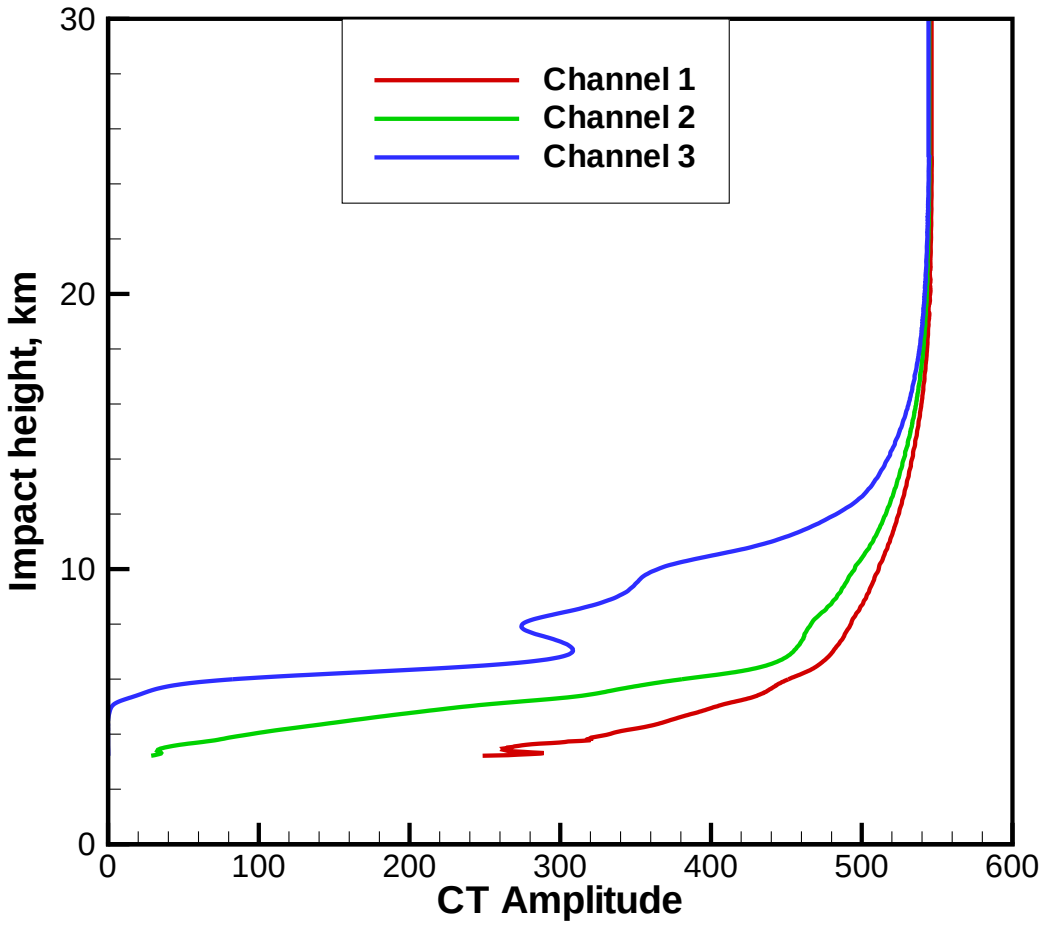

Figure 16: Simulated occultation event at UTC 00:00, September 06, 2007, 10.06°S 19.99°E. CT amplitudes for 9.7, 17.25, and 22.6 GHz.

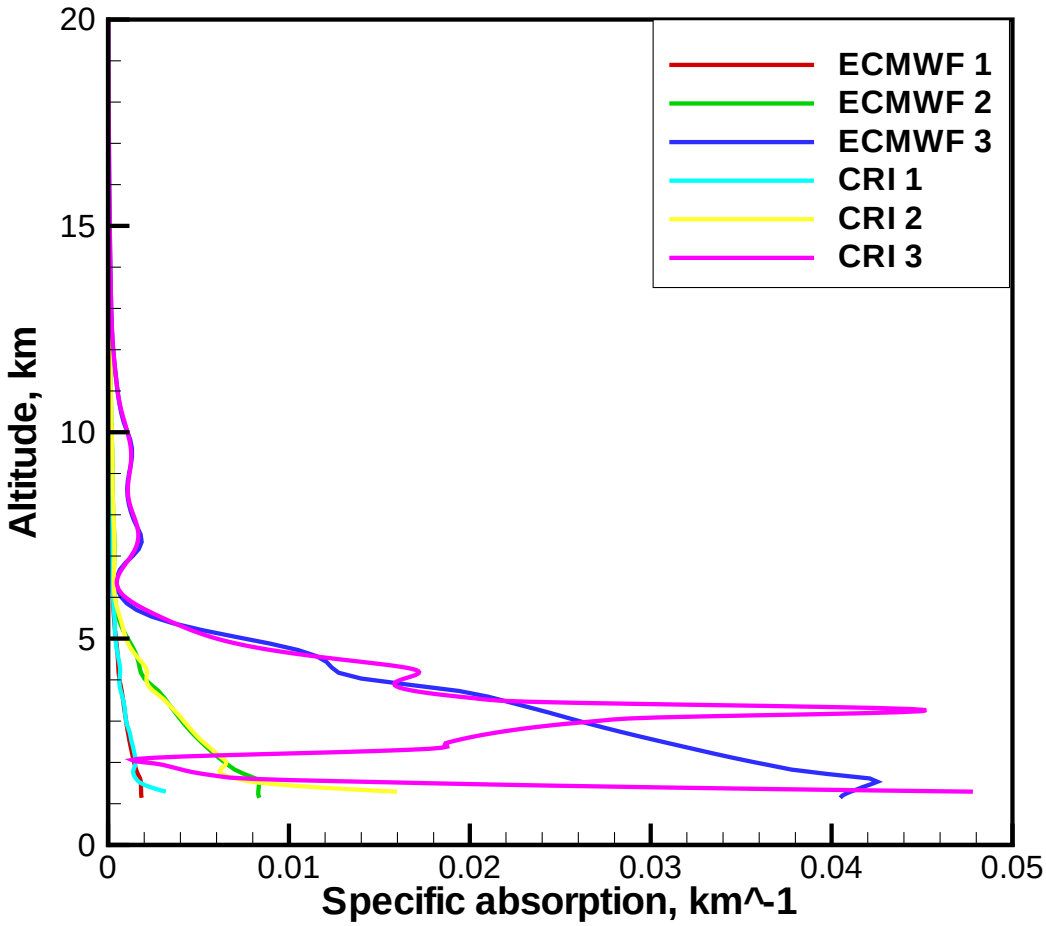

Figure 17: Simulated occultation event at UTC 00:00, September 06, 2007, 10.06°S 19.99°E. Retrieved (CRI) and reference (ECMWF) specific absorption for 9.7, 17.25, and 22.6 GHz.

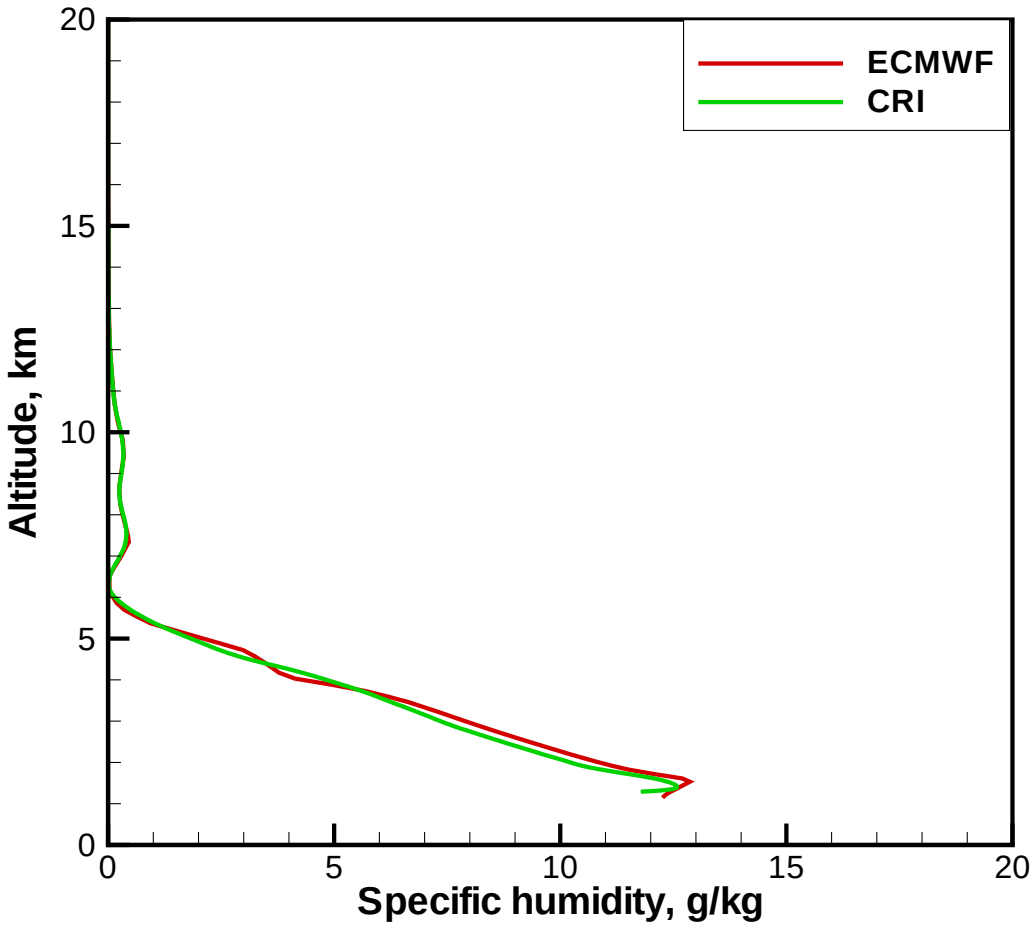

Figure 18: Simulated occultation event at UTC 00:00, September 06, 2007, 10.06°S 19.99°E. Retrieved (CRI) and reference (ECMWF) specific humidity for 9.7, 17.25, and 22.6 GHz.

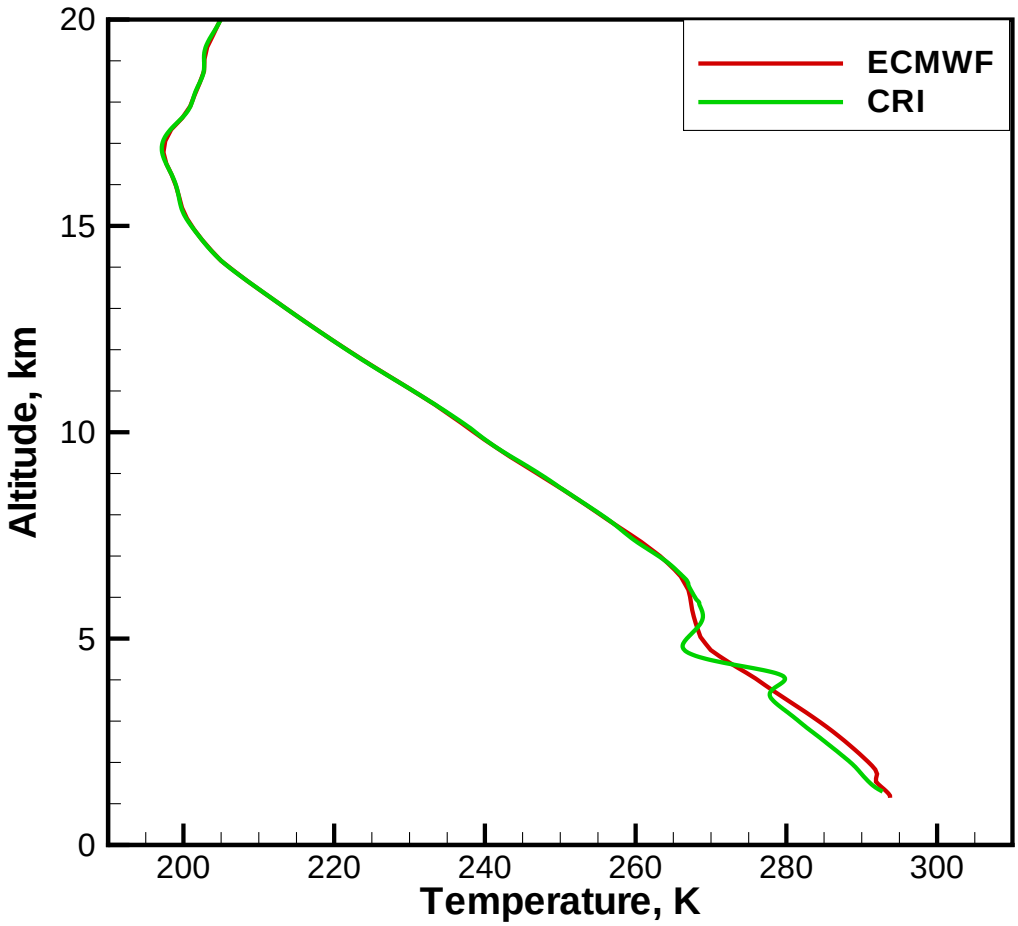

Figure 19: Simulated occultation event at UTC 00:00, September 06, 2007, 10.06°S 19.99°E. Retrieved (CRI) and reference (ECMWF) temperature for 9.7, 17.25, and 22.6 GHz.

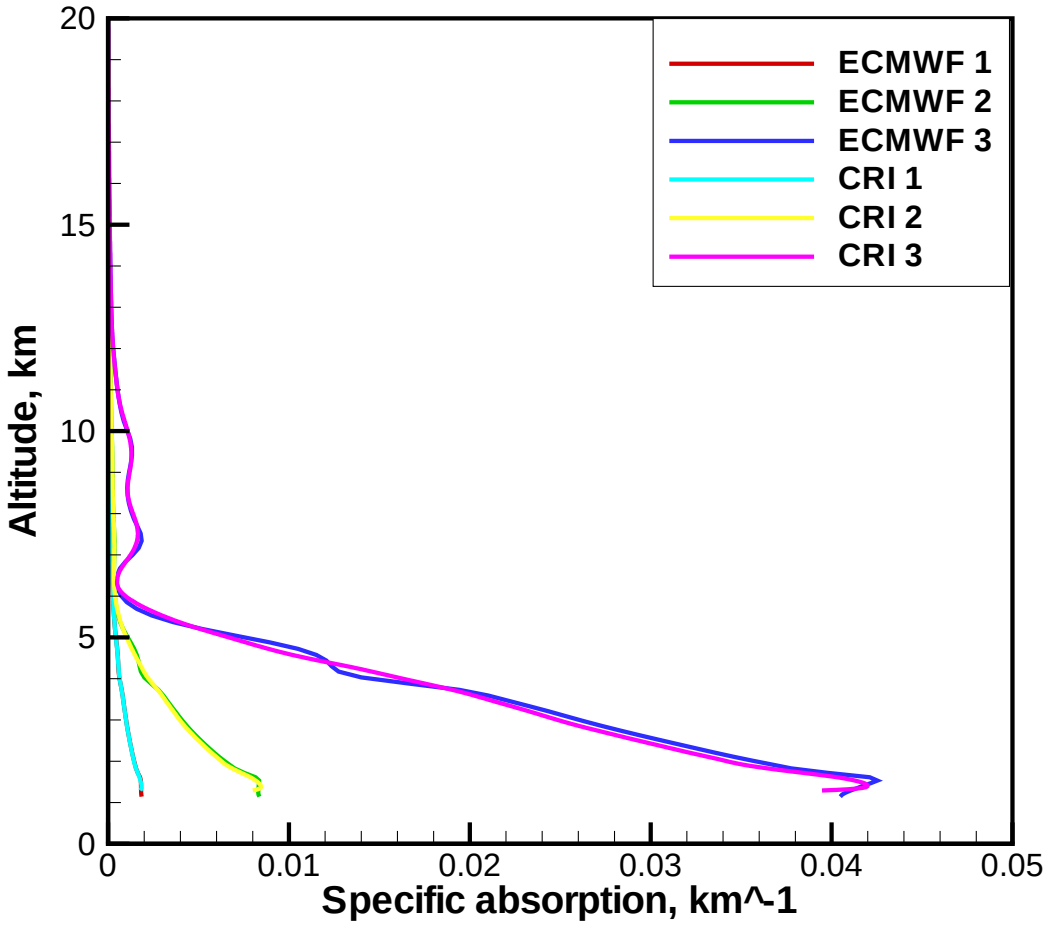

Figure 20: Simulated occultation event at UTC 00:00, September 06, 2007, 10.06°S 19.99°E. Specific absorption computed from retrieved temperature and humidity (CRI) and reference specific (ECMWF) for 9.7, 17.25, and 22.6 GHz.

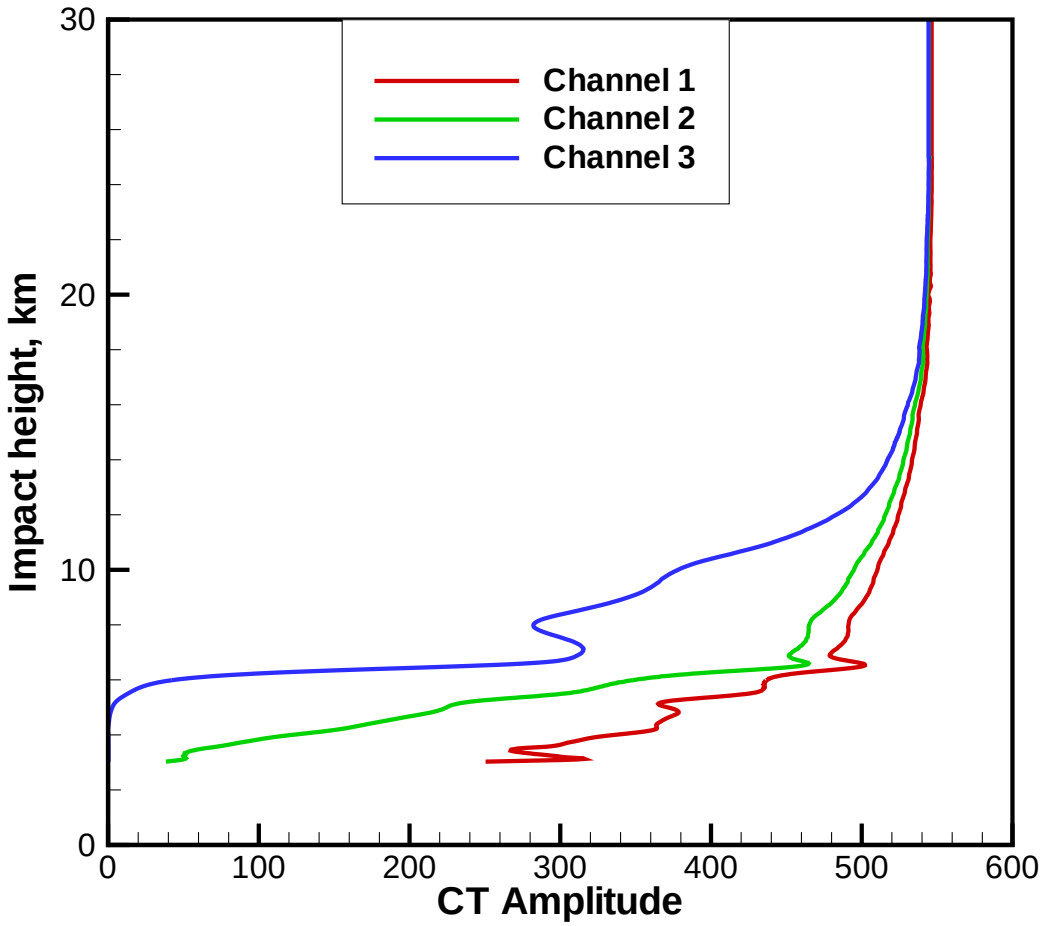

Figure 21: Simulated occultation event at UTC 00:00, September 06, 2007, 10.06°S 19.99°E. Simulation with account for horizontal gradients. CT amplitudes for 9.7, 17.25, and 22.6 GHz.

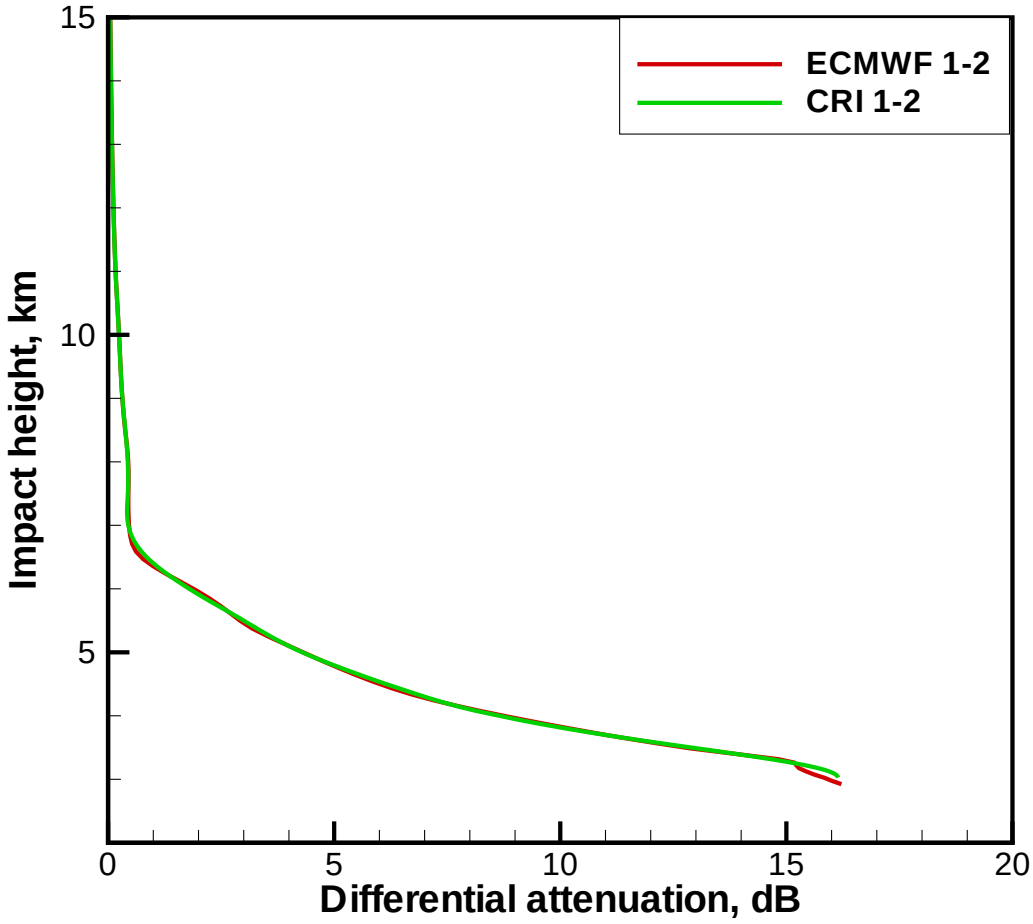

Figure 22: Simulated occultation event at UTC 00:00, September 06, 2007, 10.06°S 19.99°E. Simulation with account for horizontal gradients. Retrieved (CRI) and reference (ECMWF) Differential attenuation between channels 1 and 2 (9.7 and 17.25 GHz).

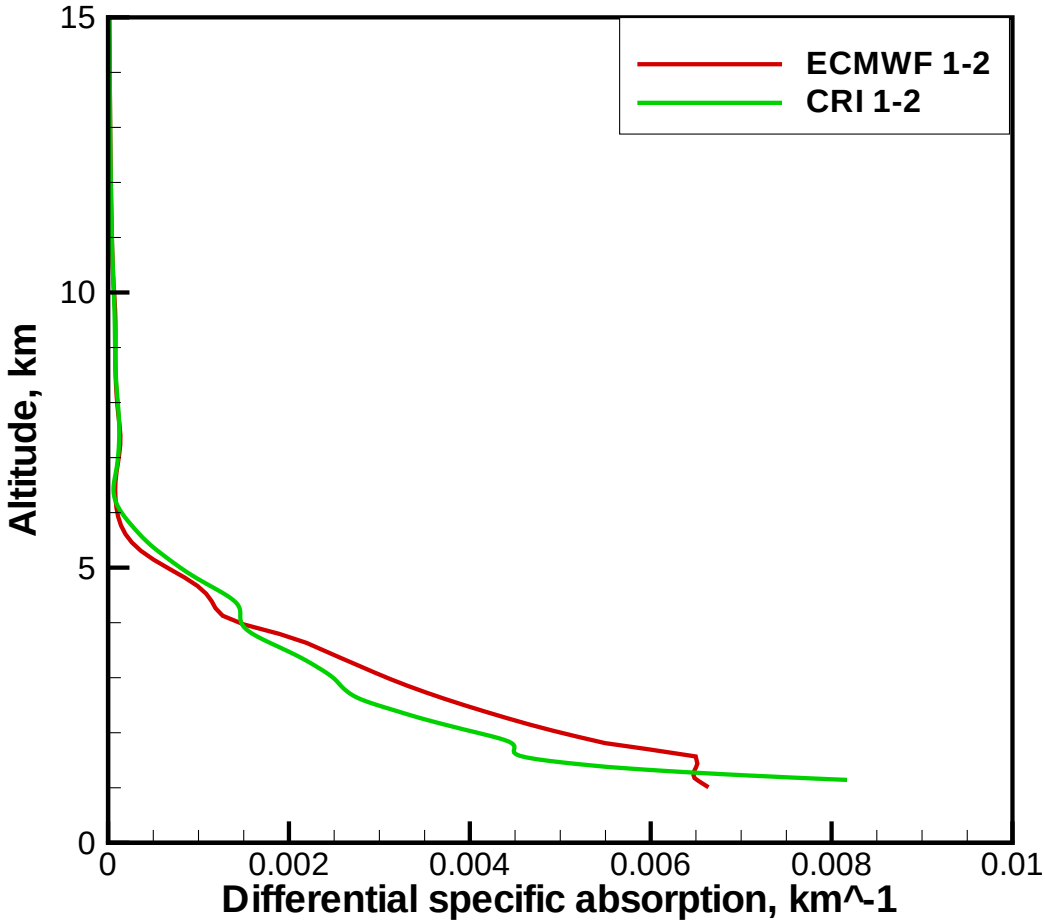

Figure 23: Simulated occultation event at UTC 00:00, September 06, 2007, 10.06°S 19.99°E. Simulation with account for horizontal gradients. Retrieved (CRI) and reference (ECMWF) Differential specific absorption between channels 1 and 2 (9.7 and 17.25 GHz).

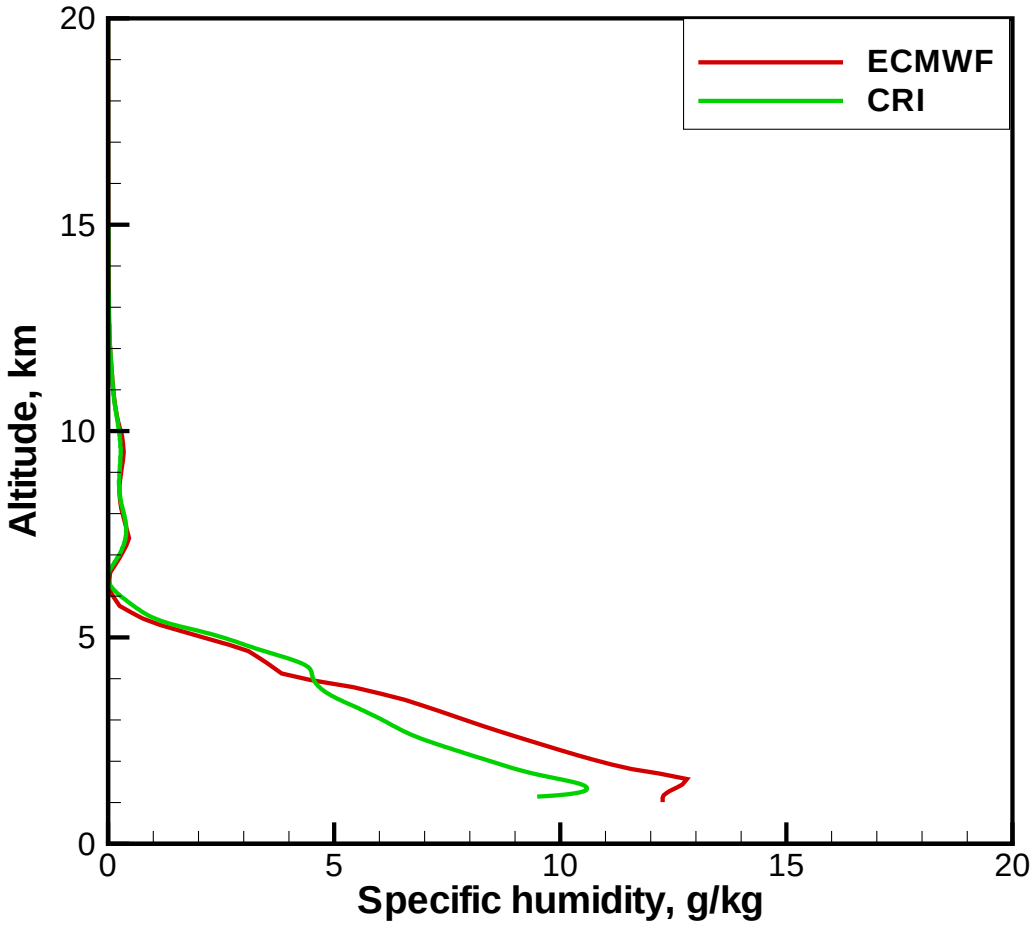

Figure 24: Simulated occultation event at UTC 00:00, September 06, 2007, 10.06°S 19.99°E. Simulation with account for horizontal gradients. Retrieved (CRI) and reference (ECMWF) specific humidity for 9.7, 17.25, and 22.6 GHz.

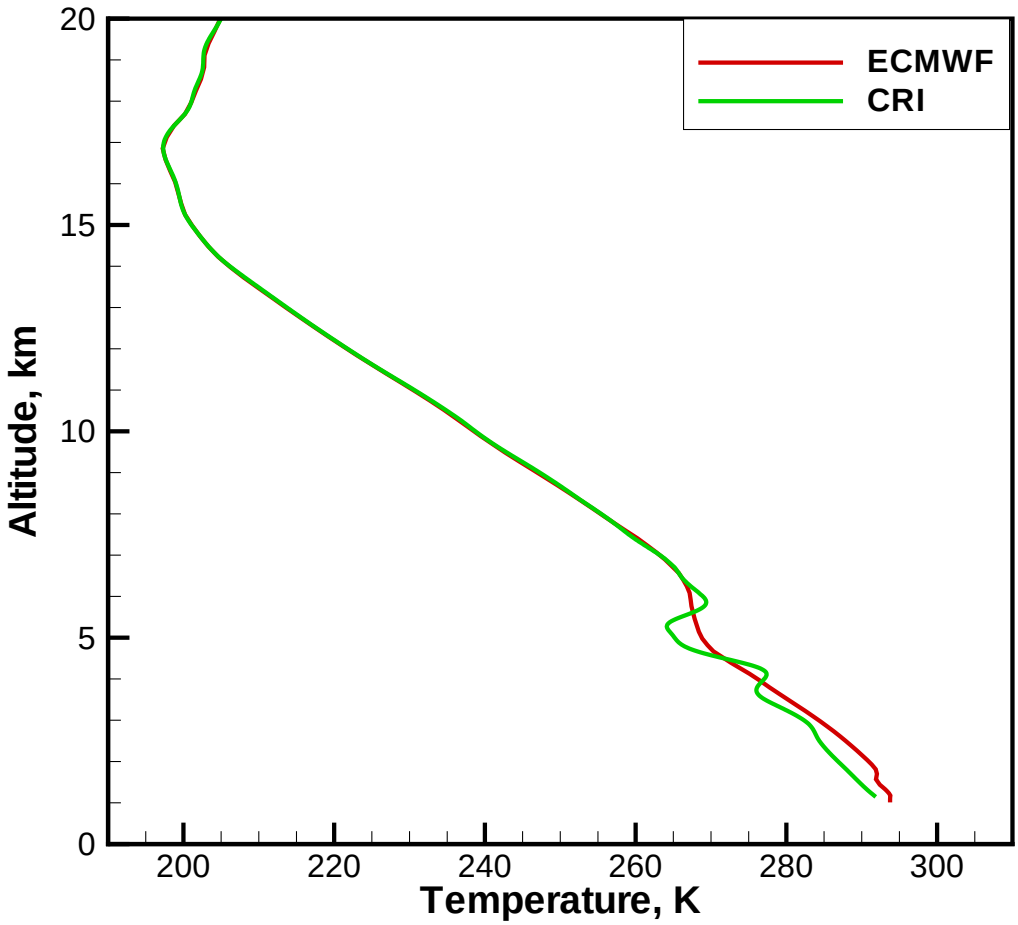

Figure 25: Simulated occultation event at UTC 00:00, September 06, 2007, 10.06°S 19.99°E. Simulation with account for horizontal gradients. Retrieved (CRI) and reference (ECMWF) temperature for 9.7, 17.25, and 22.6 GHz.